Molecular Cancer

RESEARCH

Open Access

C1Q^{+} TPP1^{+} macrophages promote colon cancer progression through SETD8-driven p53 methylation

Veronica Veschi[1,2*†], Francesco Verona[3†], Sebastiano Di Bella[1], Alice Turdo[3], Miriam Gaggianesi[1], Simone Di Franco[1], Laura Rosa Mangiapane[3], Chiara Modica[1], Melania Lo Iacono[3], Paola Bianca[3], Ornella Roberta Brancato[1], Caterina D'Accardo[3], Gaetana Porcelli[3], Vincenzo Luca Lentini[4], Isabella Sperduti[5], Elisabetta Sciacca[6], Peter Fitzgerald[7], David Lopez-Perez[8], Pierre Martine[8], Kate Brown[8], Giuseppe Giannini[2,9], Ettore Appella[8], Giorgio Stassi[1*†] and Matilde Todaro[3,10†]

Abstract

Background In many tumors, the tumor suppressor *TP53* is not mutated, but functionally inactivated. However, mechanisms underlying p53 functional inactivation remain poorly understood. SETD8 is the sole enzyme known to mono-methylate p53 on lysine 382 (p53^{K382me1}), resulting in the inhibition of its pro-apoptotic and growth-arresting functions.

Methods We analyzed SETD8 and p53^{K382me1} expression in clinical colorectal cancer (CRC) and inflammatory bowel disease (IBD) samples. Histopathological examinations, RNA sequencing, ChIP assay and preclinical in vivo CRC models, were used to assess the functional role of p53 inactivation in tumor cells and immune cell infiltration.

Results By integrating bulk RNAseq and scRNAseq approaches in CRC patients, SETD8-mediated p53 regulation resulted the most significantly enriched pathway. p53^{K382me1} expression was confined to colorectal cancer stem cells (CR-CSCs) and C1Q^{+} TPP1^{+} tumor-associated macrophages (TAMs) in CRC patient tissues, with high levels predicting decreased survival probability. TAMs promote p53 functional inactivation in CR-CSCs through IL-6 and MCP-1 secretion and increased levels of CEBPD, which directly binds SETD8 promoter thus enhancing its transcription. The direct binding of C1Q present on macrophages and C1Q receptor (C1QR) present on cancer stem cells mediates the cross-talk between the two cell compartments. As monotherapy, SETD8 genetic and pharmacological (UNC0379) inhibition affects the tumor growth and metastasis formation in CRC mouse avatars, with enhanced effects observed when combined with IL-6 receptor targeting.

†Veronica Veschi and Francesco Verona contributed equally to this work.

†Giorgio Stassi and Matilde Todaro senior authors.

*Correspondence:
Veronica Veschi
veronica.veschi@uniroma1.it
Giorgio Stassi
giorgio.stassi@unipa.it
Full list of author information is available at the end of the article

Conclusions These findings suggest that p53^{K382me1} may be an early step in tumor initiation, especially in inflammation-induced CRC, and could serve as a functional biomarker and therapeutic target in adjuvant setting for advanced CRCs.

Keywords SETD8, P53^{K382me1}, Cancer stem cells, C1Q^{+} TPP1^{+} macrophages, IBD, CRC

Graphical Abstract

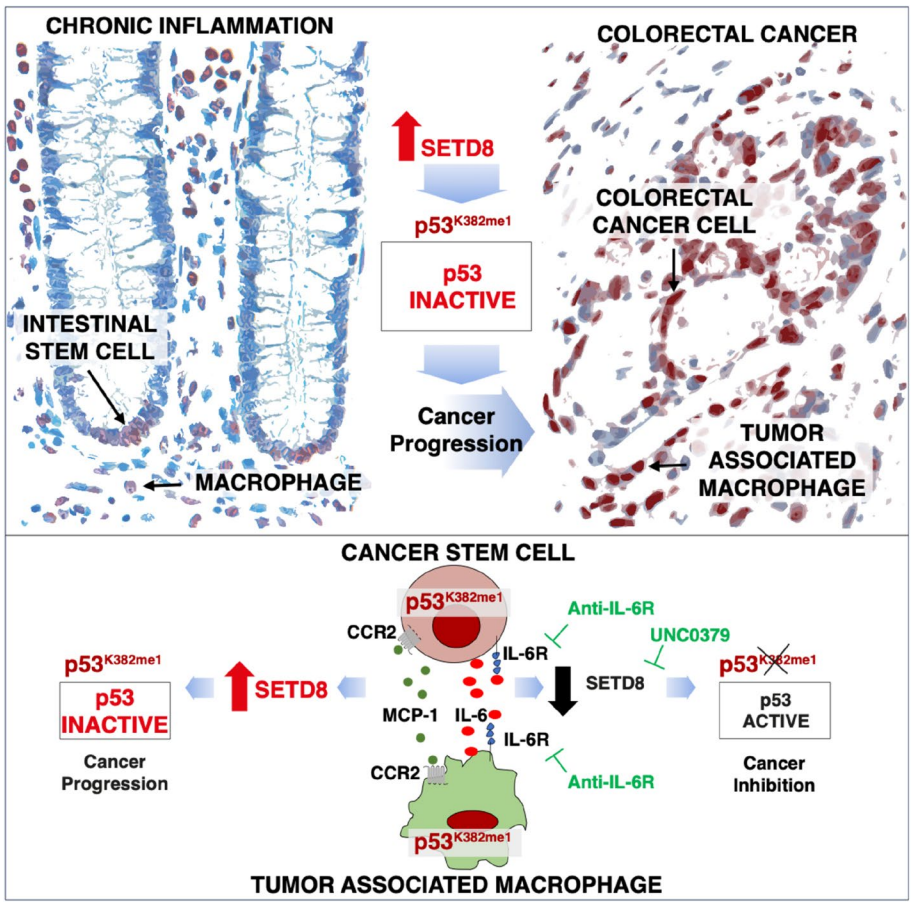

Background

Colorectal cancer (CRC) is the third leading cause of cancer-related mortality in Western countries, due to the limited efficacy of existing conventional therapies [1]. The tumor suppressor *TP53* (p53) is the most frequently mutated gene in human cancers, exceeding a 50% prevalence [2]. In numerous tumors, including CRC, p53 can be functionally impaired even without mutations. Sporadic CRCs are those that arise without discernible contributions from the germline or notable family history of the disease and encompass about two-thirds of all diagnosed CRC cases. Mutations of p53 frequently occur late in the disease progression, and initially, 50–60% of cases exhibit wild-type p53 ($p53^{WT}$). However, in colitis-associated CRC, functional inactivation of p53 often represents an early event in tumorigenesis [3]. The restoration of p53 activity in preclinical cancer models leads to tumor cell death, indicating a promising therapeutic approach for tumors retaining $p53^{WT}$ [4]. Despite this potential, the mechanisms underlying p53 functional inactivation in many tumors remain poorly understood, and p53 reactivation therapies are not yet commonplace in clinical practice. Unveiling further mechanisms of functional p53 inactivation and deepening our understanding of the anticancer effects resulting from restored p53 activity is crucial, not only in cancer cells but also within host cells

infiltrating the tumor microenvironment. This is essential for optimizing the application of this strategy in therapeutic contexts within clinical settings.

Recently, we identified SETD8 as a crucial suppressor of p53 activity in neuroblastoma (NB) [5]. SETD8, a histone methyl transferase (HMT), mono-methylates histone H4 on lysine 20 ($H4^{K20me1}$) and plays a critical role in regulating DNA replication and chromosome condensation during mitosis [6]. SETD8 is overexpressed and exhibits oncogenic functions across various cancer types, including bladder, pancreatic, small and non-small cell lung cancers, chronic myelogenous leukemia and hepatocellular carcinoma [7]. In NB, focal copy number gains of Chr12q24, a region that includes *KMT5A* (SETD8), contribute to the observed overexpression of SETD8 [8]. In addition to histone H4, SETD8 also methylates non-histone targets of the p53 pathway, including p53 itself and NUMB. In particular, it is the sole known mono-methyltransferase that mono-methylates p53 on lysine 382 ($p53^{K382me1}$), which results in the inhibition of p53 pro-apoptotic and growth-arresting functions [9]. Additionally, $H4^{K20me1}$ has been implicated in regulating the expression of the p53 family member p73 and in modulating the DNA damage response through 53BP1 [10–12].

Inflammatory conditions affecting the lower gastrointestinal tract, such as ulcerative colitis (UC) and Crohn's disease (CD), contribute to the development of CRC. Persistent inflammatory stimuli in this context may further promote tumor progression and metastasis. The immune microenvironment plays a significant role in the development of chemo-resistant CRC, with particular involvement of macrophage-derived interleukins, such as IL-6 [13]. While the immune microenvironment of Consensus Molecular Subtype-1 (CMS-1) CRCs plays mainly an anti-tumor role, the immune microenvironment of CMS4, which is characterized by the presence of Treg, T helper 17, myeloid-derived suppressor cells and tumor-associated macrophages, exerts a pro-inflammatory and tumor-promoting function [14]. The presence of immunosuppressive cytokines like IL-23 and IL-17 establishes a link between CMS4 cancers to colitis-associated colorectal carcinoma. In this type of CRC, p53 inactivation occurs early in the transformation to dysplasia, in this type of CRC, distinguishing it from CMS2 precursor lesions, where the loss of p53 tumor suppressor function occurs late in the adenoma-to-carcinoma sequence [15].

Epigenetic regulators are known to significantly affect epigenetic reprogramming of cancer stem cells (CSCs) [16]. The tumor suppressor gene PRDM, recognized as a p53 response gene, plays a crucial role in silencing stem cell-related genes and inhibiting the proliferation of human colon tumor organoids. This supports the hypothesis that p53 serves as a key regulator of stemness and epigenetic reprogramming in colorectal CSCs (CR-CSCs) [17].

p53 plays an important role in the differentiation of macrophages from monocytes, and disrupting p53 functions has a profound impact on this developmental process [18]. Activation of p53 is also pivotal in M1 polarization, blocking the expression of M2 genes even in macrophages already polarized towards the M2 phenotype [19]. Notably, the acetylation of p53 enhances this process [20]. Indeed, as p53 actively suppresses M2 macrophage polarization, the shift to M2 pro-tumoral macrophages requires mutation or functional inactivation of p53 [19]. M1 macrophages express higher p53 levels than M2 macrophages and follow a classical p53 activation pathway, activating p21 [19]. The acetylation of p53 by p300/CBP is essential for polarizing macrophages to the M1 phenotype, and inhibition of p300/CBP abolishes M1 polarization [20]. The specific residue of p53 requiring acetylation remains unknown. Conversely, M2 macrophages express lower levels of p53 than M1 and their p53 undergoes extensive ubiquitylation [19]. The status of p53 in macrophages plays a crucial role in CRC tumorigenesis. In CRC murine models, p53 deletion in macrophages significantly increases the number of adenomas and promotes tumor progression [21]. Thus, inactivation of p53 appears to be an early and critical process that facilitates tumor formation. The mechanisms of p53 inactivation in macrophages have not yet been elucidated. Tumor-associated macrophages (TAMs) exhibit enhanced expression of methyltransferases before undergoing epigenetic changes [22]. However, the effects of p53 methylation and histone methylation in macrophages are both still incompletely understood. Therefore, a better understanding of SETD8 biology and its regulatory functions in the p53 pathway in CRC cells and host cells may lead to the development of more effective therapeutic strategies with reduced side effects.

Methods

Cell lines and colorectal cancer sphere cells

SY5Y human neuroblastoma cells, HCT116 human colorectal carcinoma cells, LOVO human colorectal adenocarcinoma cells, CRL-1790 normal human colon cells, CRL-1831 normal human colon cells, THP-1 (THP1) human leukemic monocytes/macrophages, were obtained from ATCC and cultured at 37 °C in a humidified 5% CO2 atmosphere as suggested by the supplier.

Colorectal cancer sphere cells (CR-CSphCs) were freshly isolated from 11 human primary tumor specimens of CRC patients (#3, #7, #8, #9, #12, #14, #18, #21, #22, #23, #24) provided by the University Hospital "P. Giaccone", in accordance with the ethical policy of the

Institutional Committee for Human Experimentation (authorization CE9/2015, Policlinico Paolo Giaccone, Palermo). Clinical data of the 11 CRC patients from which CR-CSphCs were isolated, and their mutational background are reported in Table S2.

Human samples were digested with collagenase (0.6 mg/ml) and hyaluronidase (10 μg/ml). Then, CR-CSphCs were cultured in ultra-low adhesion using serum-free stem cell medium (SCM) supplemented with EGF and b-FGF as previously described (Todaro et al., 2014).

In commercially established (CE) cell lines and CR-CSphCs, mycoplasma contamination was evaluated every three months using the MycoAlert™ Plus Mycoplasma Detection Kit (Lonza) according to the manufacturer's instructions. CE cell lines and CR-CSphCs were routinely validated by short tandem repeat (STR) analysis using a multiplex PCR assay (GlobalFiler™ STR kit, Applied Biosystem) and analyzed by ABIPRISM 3130 genetic analyzer (Applied Biosystems) according to the manufacturer's instructions. CR-CSphCs were exposed to the following conditioned media (CM): CM1, derived from freshly isolated human 5×10^5 CR-CSphCs, CM2 derived from human macrophages 5×10^5 (THP1), CM3 collected upon direct interaction between freshly isolated human 2.5×10^5 CR-CSphCs #8 and 2.5×10^5 human macrophages (THP1). CMs were harvested after 48 h.

CM3 was obtained by plating 2.5×10^5 THP1 and 2.5×10^5 CR-CSphCs #8 in 4 ml of ADVANCED DMEM/F12 (Gibco) supplemented with Hepes 10 mM (Euroclone), glutamine 2 mM (Euroclone), N-acetyl-L-cysteine 1 mM (Sigma-Aldrich), N2 supplement 1X (Gibco), B27 supplement (Gibco) 1X, Nicotinamide 10 mM (Sigma-Aldrich), P/S 100 U/ml (Euroclone), Gastrin 10 nM (Sigma-Aldrich) without serum, EGF and b-FGF for 48 h in Ultra-Low Attachment Multiple Well Plate (Corning).

CR-CSphCs or THP1 cells were treated with human recombinant IL-6 (25 ng/ml), MCP-1/CCL2 (0.25 μg/ml), UNC0379 (0.5, 1, 2, 4, 8 μg/ml) and RoActemra (Tocilizumab) (2.5 μg/ml). Cytokines and inhibitors were added every 48 h to cell culture. Treatment with neutralizing antibodies targeting IL-6 (8 ng/ml) and MCP-1 (0.5 μg/ml) (R&D systems) lasted 24 h. CR-CSphCs were treated with doxycycline (1 μg/ml) and added every 48 h to cell culture.

Patient-derived tissue samples

CRC tissues were obtained at the time of resection from 11 patients (age range 47–85 years), in accordance with the ethical standards of the Institutional Committee on Human Experimentation (authorization CE9/2015, Policlinico "Paolo Giaccone", Palermo). All patients provided written informed consent. Normal colon mucosa was obtained from the histologically uninvolved resection. Clinical data of 11 CRC patients from which CR-CSphCs were isolated, are reported in Table S2.

Tissue microarray (TMA) slides of 185 CRC patients were provided National Institutes of Health (NIH). Clinical data of 185 CRC patients are reported in Table S3.

Screening Approach integrating RNAseq data and scRNAseq

The "Chromatin Modifying Enzymes" signature including 272 genes obtained from Reactome Gene set (MSigDB, C2:CP) was used to filter differentially regulated genes (DEGs) with positive fold change and p-value < 0.05 in TCGA COAD and GSE200997 dataset, comparing Normal colon mucosa vs Tumor tissues derived from CRC patients (Bulk RNAseq) and Normal Enterocytes vs CRC cells (scRNA-seq), respectively. The intersection of the two sets of genes (125 genes for Bulk RNASeq and 77 for scRNA-seq) identified a signature of 65 common genes. An Enrichment Analysis in Reactome Gene Set was performed using the 65 genes signature and the top significantly enriched pathways were sorted by p-value. Along with epigenetic regulation and chromatin remodeling, pathways related to p53 signaling were among the top significantly enriched. *KMT5A (*SETD8) came out as one gene in common in 3 out of 5 top p53-related pathways. Gene Signatures at each step of the flow chart shown in Fig. 1A is reported in Table S1.

Immunohistochemistry and Immunofluorescence

Immunohistochemical analysis was performed on 4 μm-thick paraffin-embedded sections derived from healthy colon IBD (Chron's disease and ulcerative colitis) and CRC samples as previously reported (Todaro et al., 2007) and subsequently exposed to specific antibodies against SETD8 (43AT551.86, mouse IgG1, Abcam), $p53^{K382me1}$ (Abwiz Bio, Cat# 2792), CD44v6 (2F10, mouse IgG1, R&D systems), p53 (DO7, mouse IgG2b, Santa Cruz Biotechnology), CD68 (PG-M1, mouse IgG3,κ, Dako), CD163 (10D6, IgG1, Novacastra Leica), CK20 (Ks20.8, IgG2a, kappa, Leica Biosystems), H4 (rabbit polyclonal, Active Motif), $H4^{K20me1}$ (5E10-D8, mouse IgG1, Active Motif), REG1A (Bio Vendor, # RD172078100). Then, antigens were revealed using polymer horseradish peroxidase (HRP) conjugated antibodies (Biocare Medical) and were detected by DAB and Vulcan Fast Red chromogen. The counterstaining of nuclei was performed with aqueous hematoxylin (Sigma-Aldrich) as described in the standard protocol. H&E stainings were performed using standard protocols.

Immunofluorescence analysis on tissues derived from IBD and CRC-patients was performed as previously described (Todaro et al., 2007), and incubated overnight

at 4 °C to antibodies against $p53^{K382me1}$ (Abwiz Bio, Cat# 2792), CD44v6 (2F10, mouse IgG1, R&D systems), SETD8 (43AT551.86, mouse IgG1, Abcam), CD68 (PG-M1, mouse IgG3,κ, Dako), TPP1 (2E12, mouse IgG2bκ, Sigma-Aldrich), C1Q (Jl-1, mouse IgG2b, Thermofisher Scientific), FCN1 (Abcam, Cat# ab223712), C1QR (Sigma Life Science, Cat# HPA009300), CK20 (Ks20.8, IgG2a, kappa, Leica Biosystems), Ki-67 (D3BS, Rabbit IgG, Cell Signaling), $H4^{K20me1}$ (Active Motif, Cat# 39,727), CD163 (10D6, IgG1, Novacastra Leica), CD4 (MT310, IgG1, kappa, Dako), CD8 (C8/144B, IgG1, kappa, Dako), CD15 (C3D-1, mouse IgM, Santa Cruz Biotechnology), CD20 (D-10, mouse IgM, Santa Cruz Biotechnology), LGR5 (Abgent, Cat# AP2745f). Then, cells were labeled with secondary antibodies (Invitrogen) and the nuclei were counterstained using Toto-3 iodide (Thermo Fisher). Cell quantitation was performed by ImageJ Software analysis.

Tissue microarray (TMA) slides of 185 CRC patients were exposed to specific antibodies against SETD8, $p53^{K382me1}$, p53 DO7, and CD44v6, examined microscopically by three independent observers, and stratified according to the $p53^{K382me1}$ expression into 4 classes based on $p53^{K382me1}$ presence in tumor tissue (Tum ±) and/or immune cell infiltration (Inf ±). In the TMAs of 185 CRC patients, the expression levels of SETD8 and $p53^{K382me1}$ were evaluated as positive cell number < 0 (low) and > 0 (high), and the mutational status of p53 was evaluated by p53 DO7 antibody staining as positive cell number < 0 (WT) and > 0 (MUT), as reported in Table S3.

Western blot

Human cell lines and CR-CSphCs were lysed in ice-cold lysis buffer (Tris–HCL 10 mM, NaCl 50 mM, sodium pyruvate 30 mM, NaF 50 nM, ZnCl2 5 μM, triton 1, sodium orthovanadate 0.1 nM, sodium butyrate 10 mM and PMSF 1 mM) containing protease and phosphatase inhibitors (Sigma-Aldrich). Histone proteins were extracted using EpiQuik Total Histone Extraction Kit following the manufacturing instructions (Epigentek #OP-0006–100). The extracted proteins were loaded in SDS-PAGE gels and blotted on nitrocellulose membranes. Membranes were incubated with 5% non-fat dry milk and 0.1% Tween 20 in PBS for 1 h at room temperature. Then, primary antibodies against SETD8 (43AT551.86, mouse IgG1, Abcam), $p53^{K382me1}$ (Abwiz Bio, Cat# 2792), p53 (DO-1, mouse IgG2a, Santa Cruz Biotechnology), p21 Waf/Cip (DCS60, mouse IgG2a, Cell Signaling Technology), β-actin (8H10D10, mouse IgG2b, Cell Signaling Technology), $H4^{K20me1}$ (5E10-D8, mouse IgG1, Active Motif) and H4 (rabbit polyclonal, Active Motif), were added over night. For the revealing were used anti-mouse or anti-rabbit HRP-conjugated (goat IgG; Thermo Fisher Scientific) and detected by Amersham imager 600 (GE Healthcare). Proteins were normalized on β-actin level and quantified by ImageJ software.

Flow cytometry and cell cycle analysis

CD206 (DCN228, mouse IgG1κ, Miltenyi Biotech), CD163 (REA812, human IgG1, Miltenyi Biotech), CD192 (REA538, human IgG1, Miltenyi Biotech), SOX2 (245,610, Mouse IgG2a, BD), CD133 (AC141, mouse IgG1, Miltenyi Biotech), NANOG (N31-355, Mouse IgG1, κ BD), CD68 (REA886, human IgG1, Miltenyi Biotech), IL-6 (REA1037, human IgG1, Miltenyi Biotech) expression was evaluated on THP1 cells and on CR-CSphC#8 transduced with pTRIPZ inducible lentiviral non-silencing shRNA control (ns shRNA, Dharmacon) or human SETD8 shRNA (shSETD8, Dharmacon) plasmids. THP1 cells were stimulated with LPS (Thermo Fisher Scientific) and Brefeldin A (Thermo Fisher Scientific) to stain IL-6, according to manufacturer's instructions. For intracellular staining, cells were fixed with 2% PFA for 30 min at room temperature and permeabilized with PBS and 0,1% TRITON-X 100 for 15 min at room temperature. Antibodies and their isotype controls were incubated for 30 min at 4 °C and then analyzed by BD FACs Lyric flow cytometer (BD Clinical system, BD Bioscience).

The percentage of apoptotic cells was evaluated in CR-CSphCs#8 and #24 treated with vehicle or UNC0379 (2 μM) for 24 h and 72 h by Annexin V staining (BD Bioscience) according to manufacturer's protocol.

For cell cycle analysis, CR-CSphC#8 treated with DMSO or UNC0379 (2 μM) for 48 h were incubated with 1 ml of Nicoletti Buffer (0.1% of Sodium citrate, 0.1% of Triton x-100, 50 μg/ml of Propidium Iodide,10 μg/ml of RNase solution) in the dark at 4 °C overnight. DNA content was evaluated by BD FACs Lyric flow cytometer (BD Clinical system, BD Bioscience). The overall obtained data were analyzed by FlowJo software.

Cytokines quantification

THP1- and CR-CSphC#8-released cytokines involved in tumor inflammation, cell proliferation and immune response processes were quantified using the Bio-Plex ProTM Human Chemokine/Cytokine 40-plex Assay (Bio-Rad). Cytokines released in conditioned media CM1, CM2 and CM3 harvested after 48 h and generated as described above, were evaluated. Raw data were analyzed by Bio-Plex Software (Bio-Rad).

Real-time PCR

TRIzol™ Reagent (Thermo Fisher) was used to extract total RNA and 1 μg of total RNA was retrotranscribed according to the manufacturing protocol High-Capacity

cDNA Reverse Transcription Kit (Applied Biosystem, Cat# 4,368,814). The expression analysis of genes related to p53 signaling and EMT- Wnt and stemness pathways was evaluated using PrimePCR designed custom panels (Bio-Rad). The expression levels of the relative mRNA were normalized with the endogenous control (GAPDH) and calculated using the comparative Ct method ($2^{-\Delta\Delta Ct}$). High-Capacity cDNA Reverse Transcription Kit (Applied Biosystems) was used for RNA retro transcription for Real-time PCR. Quantitative Real-time PCR analysis was performed in a SYBR Green Master Mix (Qiagen, 1,054,586) using primer sequences indicated in Table S4.

Chromatin Immunoprecipitation and qPCR

ChIP-qPCR analysis of *KMT5A* (SETD8) promoter was performed as follows. ChIP analysis was performed in THP1 cells untreated and treated with IL-6 for 90 min by using Active Motif ChIP-IT High Sensitivity #53,040 protocol, followed as published. Samples were sheared at 25% 5X 20 s on 30 secs off. Shearing efficiency was assessed on EZ-gel 1%. Equal amounts of sheared DNA were used in IgG control and C/EBPδ samples. C/EBPδ Antibody Abcam # ab245214 – 4ug total used, and IgG rabbit Abcam #ab171870 was used. Samples were eluted in 200ul.

qPCR was run on BioRad CFX Duet using BioRad 2X SYBR green Master mix, 2.5 µM primers targeting *KMT5A* (SETD8). Samples were run in triplicate. $^{\Delta\Delta Ct}$ was used to calculate fold enrichment of C/EBPδ at the SETD8 promoter over IgG control. In details, the precipitated genomic DNA was analyzed by qPCR with the following primers for *KMT5A* (SETD8) and *CCL2* (MCP-1):

SETD8_F ATC AAA CTG CTG GAG AGG TCG
SETD8_R GAT CTG GGA CTT CCG GTT CTC
MCP1_p1FCACTAACTGAGGCCATGAACAGGT TAGTG
MCP1_p1RGCAAACCAGCACAAATGTAGCC
MCP1_p2FTTGGAATGTGGCCTGAAGGT
MCP1_p2RAGGGTTATTTTTAAGGATTCTGC TTTC
MCP1_p3FCGTTCTGGGAGCTAGAGGAGGAACG
MCP1_p3RCTCTCCACCTGGGTGCCTATTC

MCP1 three sets of primers were used as positive control. The fold enrichment method used to calculate the enrichment of the KMT5A (SETD8) promoter is detailed here: https://www.thermofisher.com/us/en/home/life-science/epigenetics-noncoding-rna-research/chromatin-remodeling/chromatin-immunoprecipitation-chip/chip-analysis.html. A complete list of antibodies and reagents utilized, and their identifiers are listed in Table S7, a key resources table.

RNA-seq analysis

RNA was extracted using the Qiagen RNeasy mini kit including the optional DNase clean-up step. Samples were analyzed for QC using the RNA ScreenTape station and RIN scores were measured. 1 µg of total RNA was used for the construction of sequencing libraries.

For the IL6-CM3 experiment, 12 RNA-seq samples were pooled and sequenced on NovaSeq 6000 SP using Illumina Stranded Total RNA Prep, Ligation with Ribo-Zero Plus and paired-end sequencing. The samples had 59 to 194 million pass filter reads with more than 91% of bases above the quality score of Q30.

Reads of the samples were trimmed for adapters and low-quality bases using Cutadapt before alignment with the reference genome (hg38) and the annotated transcripts using STAR (version 2.7.0.f).

Sequence alignments and gene expression quantification

For all types of sequencing data, the MultiQC (version 1.13, https://multiqc.info/) software was used to assess the quality of raw sequencing data. The reads were aligned to the Human Genome Reference Consortium build 38 (GRCh38) using STAR (version 2.7.0f) and the gene expression quantification were performed RSEM (version 1.3.1). The average mapping rate of all samples was 90%. Unique alignment is above 77%. Regarding unmapped reads there were 7.89 to 11.03%. The mapping statistics were calculated using Picard software (version 2.18.26). The samples had 0.01% ribosomal bases. Percent coding bases were between 27–36%. Percent UTR bases were 20–27%, and mRNA bases were between 48–63%. Library complexity was measured in terms of unique fragments in the mapped reads using Picard's MarkDuplicate utility. Not duplicate reads were 73–80%. In addition, the gene expression quantification analysis was performed for all samples using STAR/RSEM tools.

The raw counts file was analyzed in R. Firstly, the datasets were filtered to keep the genes with at least 0.5 counts per million in at least 2 samples. Then library sizes were compared to assure that they were similar. Then, the differential expression analysis was performed with edgeR. The gene list ranked by decreasing logFC (log2 fold-change) was employed for gene set enrichment analysis (GSEA) with the clusterprofiler package. Significantly enriched pathways were furtherly verified by GSEA software (Broad Institute, version 4.2.3).

Differential expression analysis and gene set enrichment analysis

Differentially expressed genes (DEGs) analysis was conducted by R with edgeR (version 3.42.4) library based on the following criteria: (1) adjusted $P < 0.05$ and (2) $Log_2FC \geq 1.5$.

189 differentially expressed genes were found. Gene set enrichment analysis (GSEA) was performed by using R library msigdbr (version 7.5.1) and querying the Hallmark (H) and Reactome sub-category of canonical pathway (C2:CP), which includes 1654 pathways. Pathways statistically significant with p-value < 0.05 were selected. Genes involved in TNFa via NFKB, INF alpha-response and EMT pathways were extracted from Reactome signatures. Heatmaps were plotted using R library ggplot2 (version 3.4.4) and ComplexHeatmap (version 2.16.0).

scRNA-seq data analysis

The raw count file was downloaded from the NCBI Gene Expression Omnibus with the accession code GSE200997. The total number of cells analyzed is 18,273 cells in normal colon mucosa derived from 8 CRC patients and 31,586 cells in the tumor tissues derived from 16 CRC patients. The analysis was performed with R using Seurat package (version 5). Genes expressed in less than 3 cells as well as cells expressing less than 200 genes, more than 5000 genes, or with an enrichment of more than 30% in mitochondrial were removed from the analysis for quality purposes. Data was log-normalized, variable genes were selected through variance stabilizing transformation (VST), and data was scaled. A principal component analysis (PCA) was performed, and the top 50 principal components were employed in a uniform manifold approximation and projection (UMAP) for dimension reduction. The clustering was performed using the *FindClusters* function, which uses the k-nearest neighbors (KNN) algorithm to construct the shared nearest neighbors (SNN) graph. Modularity optimization was performed using *Louvain* algorithm.

The *FindMarkers* function was used to identify the main cell type and differentially expressed markers in each cluster. Genes with a positive average expression of twofold or higher in that cluster than in the other clusters were employed. Besides, known markers for different cell types were also used in cell type identification: Epithelial cells (EPCAM, KRT8, KRT18), normal enterocytes (FABP1), goblet cells (MUC2, SPINK4), normal Paneth cells (LYZ, CD24, MMP7), metaplastic or inflammatory Paneth cells (REG1A), tuft cells (LRMP, SH2D6), endothelial cells (CLDN5, VWF, PECAM1), fibroblasts (COL1A1, COL1A2, DCN), mast cells (GATA2, TPSAB1,TPSB2), T cells (CD3D, CD3E, CD3G), Th cells (CD4), naïve T cells (SELL, CCR7), Th17 (IL17A, KLRB1, RORC, IL4I1), Tc cells (CD8A, CD8B), B cells (CD79A, CD79B), plasma cells (MZB1, JCHAIN), centrocytes (RGS13), fresh centroblasts (TCL1A, IGHD, IGHM), centroblasts that underwent class switch recombination (CD27, TNFRSF13B, IGHA1, IGHA2). A heterogeneous cluster of myeloid cells was further sub-clusterized with the *FindSubCluster* and *FindMarkers* functions to identify the differentially expressed genes in each subcluster.

UMAP was employed to group projected cells and default settings were used to visualize monocle results using data processed from Seurat and imported in Monocle3 R package.

Exocytosis and Secretion Score Calculation

To evaluate the exocytosis potential, scRNA-seq data from tumor samples were analyzed. Cell types were ranked based on the average expression levels of 18 genes associated with the exocytosis machinery (see Table S6 for the list of genes). For each gene, a ranking was generated by assigning points to cell types according to their relative expression. Cell type with the highest expression was assigned 33 points, corresponding to the total number of cell types, while the lowest-expressing cell type received 1 point. This procedure was repeated for all 18 genes, producing 18 separate rankings.

The exocytosis potential score for each cell type was calculated as the sum of its points across all rankings:

$$Exocytosis\ Potential\ Score\ Cell\ Type\ A = \sum_{i=1}^{18} Rank(i, A)$$

where i represents each of the genes listed in Table S6.

The secretion score for a cytokine, such as IL-6, in each cell type was calculated as:

$$Secretion\ Score_{IL6,A} = Expression\ IL6, A \times \left(\frac{ExoPotA}{ExoPotX}\right) \times \left(\frac{P_{A,Tumor}}{P_{A,Mucosa}}\right)$$

where:

- $\text{Expression}_{\text{IL-6, A}}$ is the average IL-6 expression level in Cell Type A,
- ExoPot_{A} is the exocytosis potential score of Cell Type A
- ExoPot_{X} is the exocytosis potential score of the cell type with the highest exocytosis potential score across all cell types
- $\text{P}_{\text{A, Tumor}}$ is the proportion of cell type A in the tumor
- $\text{P}_{\text{A, Mucosa}}$ is the proportion of cell type A in the mucosa

This approach integrates cytokine expression levels with the relative exocytosis capacity of each cell type and with the abundance of the cell type, providing a normalized measure of secretion potential that accounts for these factors.

Cell proliferation, cell migration and clonogenic assay

For cell viability assay #8, #14, #18, #21, #22, #24 CR-CSphCs treated or not with UNC0379 (0–8 range, Selleckchem) were plated 2×10^3 in ultra-low attachment 96-well plates (Corning). At 48 h, 72 h and 6 days, spheres vitality was measured at using CellTiter 96® AQueous One Solution Cell Proliferation 369 Assay (MTS, Promega), according to the manufacturer's instructions and analyzed by the GDV MPT 370 reader (DV 990 BV6). For cell proliferation CR-CSphC#8 transduced with TRIPZ inducible lentiviral nonsilencing shRNA control (ns shRNA, Dharmacon) or human SETD8 shRNA (shSETD8, Dharmacon) plasmids were plated in ultra-low attachment 96-well plates (Corning). Cell number was analyzed at 24 h, 48 and 72 h using Tecan Infinite F500. Cell migration was evaluated plating CR-CSphC#8 transduced as described above in 24 transwell 8.0 μm inserts (Corning) and at 24 h, 48 and 72 h the number of migrated cells was evaluated. For clonogenic assay CR-CSphCs (#3, #8, #22, #24) were pretreated for 72 h with UNC0379 or vehicle. Then they were plated at a clonal density of 2×10^3 cells/well on Agarose Sea Plague Agar (Invitrogen). After 21 days, colonies were stained with 0.01% Crystal Violet and counted using ImageJ Software.

Transfection, transduction and constructs

HEK-293 T cells were transfected in OPTIMEM (Gibco) supplemented by XtremeGENE HP DNA transfection reagent (Roche), with TRIPZ inducible lentiviral nonsilencing shRNA control (ns shRNA, Dharmacon) or human SETD8 shRNA (shSETD8, Dharmacon), SMARTvector Inducible Non-targeting Control (nt shRNA, Dharmacon) or human TP53 shRNA (shTP53, Dharmacon) or human C/EBPδ shRNA (shC/EBPδ, Dharmacon) plasmids in association with psPAX2 (Addgene, 12,260) and pMD2.G (Addgene, 12,259) to produce lentiviral particles. CR-CSphC#8 and THP1 cells were transduced with LENTIX-Concentrator (cat#631,232) concentrated virus in presence of 8 μg/mL of polybrene (Sigma-Aldrich). Transduced cells were treated with doxycycline (1 μg/ml, Sigma-Aldrich) for 5–10 days.

In vivo *studies*

All in vivo procedures adhered to the guidelines of the institutional animal care committee at the University of Palermo (authorization # n. 154/2017-PR, Italian Ministry of Health). Male NSG mice, aged 4–6 weeks, were procured from Charles River Laboratories. The mice were housed in a barrier facility under controlled conditions with a temperature of 22 degrees Celsius, 50% humidity, and a 12-h dark/light cycle. The mice had ad libitum access to 0.45 μm-filtered tap water provided in sterile drinking bottles and were fed with pelleted chow (Special Diets Services-811900 VRF1 (P)).

For orthotopic xenograft tumors, 1.5×10^5 CR-CSphCs #8, transduced with TRIPZ inducible lentiviral nonsilencing shRNA control (ns shRNA, Dharmacon) or human SETD8 shRNA (shSETD8, Dharmacon) in combination with p-TWEEN LUC-GFP lentiviral vectors, were resuspended in 30 μl of 1:3 stem cell medium with Matrigel (BD and injected into the ceacum of NSG mice (6 mice/group). Two weeks after the injection, doxycycline (1 mg/ml, Sigma Aldrich) was administered in the drinking water every 48 h. Tumor growth and metastasis formation were monitored every 2 weeks after the injection of XenoLight D-Luciferin (PerkinElmer) by using IVIS Spectrum (PerkinElmer Inc.). After mice sacrifice, intestine and lungs were analyzed for bioluminescent signals and included for immunohistochemical analyses.

For subcutaneous injection, 5×10^5 CR-CSphCs#8, pretreated for 24 h with UNC0379 (4 μM, Selleckchem), or transduced with ns shRNA or SETD8 shRNA or SETD8 shRNA/TP53 shRNA, alone or in combination with 5×10^5 THP1 cells, transduced with ns shRNA or SETD8 shRNA, were subcutaneously injected in the right flank of 4–6 weeks old male NSG mice (6 mice/group) in 100 μl of solution composed by 1:1 cell culture medium and Matrigel (BD). Doxycycline was added to drinking water as previously described. Tumor size was evaluated two times/week using a caliper and the volume was calculated using the formula, $V=4/3\pi\times x/2\times y/2\times z/2$. At the end of the experiments, mice were sacrificed, and tumors collected for histopathological examination.

For the migration experiments, 1.5×10^5 CR-CSphCs (#8) and 1.5×10^5 THP1 cells engineered as described above were resuspended in 30 μl of PBS and injected into the spleen of 4–6 weeks old male NSG mice (6 mice/group). Bioluminescent signal was measured after cell injection (0 min), after splenectomy (30 min) and weekly up to 5 weeks. At the end of the experiments, bioluminescence signals were measured in intestine, lungs and liver and organs were collected for histopathological examination.

For subcutaneous injection, 5×10^5 CR-CSphCs#8 transduced with ns shRNA or TP53 shRNA, alone or in combination with 5×10^5 THP1 cells, were subcutaneously injected in the right flank of 4–6 weeks old male NSG mice (6 mice/group) in 100 μl of solution composed by 1:1 cell culture medium and Matrigel (BD). Where indicated, mice were treated i.p. with RoActemra (10 mg/

kg), UNC0379 (5 mg/kg) alone and in combination 3 days/week for 3 weeks. At 4 weeks, after mouse sacrifice, organs were harvested, macroscopically analyzed, and fixed in formalin for histological analysis.

Statistical analyses

Statistical analyses were performed by R version 4.3.1 (2023–06–16) – "Beagle Scouts" free software (https://www.r-project.org/) and GraphPad Prism 10, results associated with $p < 0.05$ were considered statistically significant. Error bars in plots showed the SD from independent experiments. The statistical significance was analyzed by Student's t test, One-way ANOVA followed by Bonferroni tests, nonparametric Mann–Whitney U-test as indicated. Survival estimates were calculated by R2 database (https://hgserver1.amc.nl/cgi-bin/r2/main.cgi?open_page=login) and GEPIA dataset, by Kaplan–Meier method and survival curves were compared by log rank (Mantel- Cox) test. Statistical details of each experiment were described in the associated Figure legend. Differential expression analysis was performed using edgeR library as described above. In multivariate analysis was calculated the Hazard Ratios (HRs) for each variable by Cox Proportional hazards model. For scRNA-seq, differential analysis was performed using Seurat's *FindMarker* function. TCGA COAD samples were obtained from Xena UCSC dataset (https://xenabrowser.net/datapages/) and tumor versus normal samples expression was compared by Wilcoxon test. The ranks of DEGs were used for GSEA analysis with a published Reactome and Hallmark gene sets (MSigDB).

Results

Expression of $p53^{K382me1}$ marks CR-CSCs with high metastatic capabilities

Given the frequent occurrence of p53 mutation or inactivation at various stages of CRC tumorigenesis [23], we sought to explore whether the molecular events underlying the tumorigenic potential were influenced by the epigenetic regulation of p53. We conducted a comprehensive RNA-Seq transcriptome analysis of 454 and 16 colorectal cancer (CRC) patient datasets from The Cancer Genome Atlas (TCGA) and Gene Expression Omnibus (GEO) databases, respectively. Gene set enrichment analysis (GSEA), computed with the molecular signatures database (MSigDB) revealed 65 differentially expressed genes (DEGs), among which 14 exhibited an enrichment of genes associated with the transcriptional regulation of p53, encompassing methylation or acetylation. Beyond the regulation of the p53 signaling pathway, *KMT5A* (SETD8) emerged as one of the most significantly upregulated genes (Fig. 1A; Table S1). SETD8, is a methyltransferase that inactivates p53 by inhibiting its pro-apoptotic and growth arrest functions through the methylation of its lysine 382 ($p53^{K382me1}$) [5, 9]. In agreement with previous reports, our analysis of a large cohort of CRC patients from R2 database (Tumor colon, Marisa dataset) showed that high mRNA expression levels of p53 are negatively associated with relapse free survival (RFS), regardless of the p53 mutational status (Fig. 1B; Fig. S1A-B). Moreover, analysis across the R2 (http://r2.amc.nl/) and TCGA COAD database [24] displayed higher *KMT5A* (SETD8) mRNA expression levels in samples derived from CRC patients compared with healthy patients (Fig. 1C; Fig. S1C). To further investigate SETD8 and p53, we analyzed a cohort of 185 primary and metastatic CRCs and observed high expression levels of SETD8 and $p53^{K382me1}$ compared with healthy mucosa (Fig. 1D). Specifically, we found $p53^{K382me1}$ highly expressed in 72% of $p53^{WT}$ CRC, suggesting a common mechanism of p53 inactivation in $p53^{WT}$ CRC patients (Fig. S1D-E). Of note, while SETD8 and its canonical histone target crucial for cell cycle and mitotic progression, $H4^{K20me1}$, are widely expressed throughout the tumor sections, cells expressing $p53^{K382me1}$ are mainly located at the invasion front of the tumor (Fig. 1D; Fig. S1F-H). Given that SETD8 expression is associated with the survival of CRC cells by activating the stemness pathway through Wnt target genes [25], we investigated whether the combined expression of SETD8 and $p53^{K382me1}$ could be used to categorize CRC patients into subsets endowing aggressive behavior, regardless of p53 mutation status. Immunoblot analysis showed that 8 out of 11 colorectal cancer spheres-propagated cells (CR-CSphCs), enriched on cancer stem cells (CSCs) [26], express $p53^{K382me1}$ and at least 50% of these display a high $p53^{K382me1}$/p53 ratio (Fig. 1E; Table S2). Conversely, the established cell lines HCT116 and LOVO, characterized by a differentiated status, express barely detectable levels of $p53^{K382me1}$ despite the high levels of total p53 protein and elevated SETD8 expression, particularly when compared with normal colon mucosa (Fig. 1E-F).

We then investigated the significance of $p53^{K382me1}$ expression in cells exhibiting characteristics associated with stemness. Analysis of the cohort of 185 primary and metastatic CRCs showed that 70% of the cells expressing concomitantly $p53^{K382me1}$ and CD44v6, are prominently present at the invasive tumor front (Fig. 1G-H; Fig.S1I; Table S3). We previously demonstrated that CD44v6 demarcates a population of colorectal cancer stem cells (CR-CSCs) endowed with a high tumorigenic and metastatic potential [26]. Interestingly, $p53^{K382me1}$ expression was not confined solely to CD44v6-positive cells but was also evident in the infiltrating immune cells.

We categorized the expression of $p53^{K382me1}$ into four classes based on its presence in intratumoral tissue and/or immune cell infiltration (Fig. 1I; Fig.S1I). We found a significant negative correlation between $p53^{K382me1}$ expression, when positive in both tumor and immune cell infiltration (Tum pos/Inf pos category), and the survival probability of CRC patients (Fig. 1J-K). Of note, multivariate analysis affirmed that $p53^{K382me1}$ serves as an independent adverse prognostic factor in stage I-II-III (p-value = 0.025) and even stage IV CRC patients (p-value = 0.01) (Fig.S1J). Consistently, analysis of the cohort of 185 CRC patients showed a significant correlation between high SETD8 and $p53^{K382me1}$ expression and the high-grade (II-III) tumors (p-value < 0.00001) (Fig. S1K).

Altogether, these findings imply that the inactivation of p53 by SETD8 through the methylation of lysine 382 may contribute to the metastatic potential of CR-CSCs.

Tumor-associated macrophages promote p53 inactivation in CRC cells through IL-6 and MCP-1 secretion

The presence of $p53^{K382me1}$ in both the tumor tissue and immune infiltration compartments, along with its correlation with unfavorable prognosis, prompted us to hypothesize that the immune compartment may be associated with an aggressive phenotype within the CR-CSC subpopulation. Thus, we sought to identify the specific cell population within the immune cell compartment that expresses $p53^{K382me1}$. Immunofluorescence analysis showed that the high percentage (80%) of $p53^{K382me1}$expression levels resided in the $CD68^+$ $CD163^+$ macrophage population (TAMs M2) enriched at the budding front of tumor invasion, with an additional 40% observed in tumor inter-crypt infiltration and the corresponding healthy mucosa counterpart. Conversely, minimal expression was observed within the $CD4^+$, $CD8^+$ or $CD15^+$, $CD20^+$ populations (Fig. 2A-B; Fig. S2A-B).

The data imply that immune cell infiltration within the context of chronic immune inflammation in tumors may underlie epigenetic reprogramming.

Considering that persistent inflammatory conditions in the lower gastrointestinal tract, referred to as inflammatory bowel disease (IBD), including Crohn's disease (CD) and ulcerative colitis (UC), contribute to the development of CRC [27, 28], our investigation aimed to determine the relevance of $p53^{K382me1}$ in patients with IBD and those experiencing inflammation-induced CRC. According to the reported literature [27], p53 inactivation, as indicated by high expression levels of SETD8 and $p53^{K382me1}$ at the base of the colon crypt and in infiltrating TAMs expressing CD68, is prevalent in colorectal tissue sections obtained from IBD patients compared with those derived from healthy subjects (Fig. 2C-E; Fig.S2C-D). Remarkably, the expression of $p53^{K382me1}$ is heightened in the intestinal stem compartment and inflammatory Paneth cells, identified by LGR5 and REG1A positivity, respectively, at the basal level of partially conserved colon crypts in tissue sections derived from IBD. This expression gradually decreases in the transit-amplifying cell zone and the apical area (Fig. 2F; Fig.S2D-E).

Cross-talk between cancer cells and macrophages within the tumor microenvironment may contribute to the functional inactivation of p53. The involvement of p53

(See figure on next page.)

Fig. 1 SETD8 is highly expressed in CRC cells and $p53^{K382me1}$ is an independent prognostic factor associated with poor prognosis in CRC patients. **A** Flow chart of the methodological approach to select chromatin modifying enzymes with positive fold change and *p*-value < 0.05 overexpressed in tumors derived from CRC patients compared with healthy subjects (TCGA dataset) and enriched in CRC cells compared to normal enterocytes (scRNA-seq data from GEO, GSE 200997). The top 15 significantly enriched pathways were obtained by Enrichment Pathway Analysis based on the Reactome Gene set (Molecular Signature Database, MSigDB), utilizing msigdbR library and $p < 0.05$. Pathways related to p53 signaling are among the top significantly enriched pathways. Venn Diagram showing the common genes enriched in the top 5 p53-related pathways. **B** Relapse-free survival (RFS) analysis of TP53 expression in CRC patients from R2 database (Tumor colon, Marisa dataset). Statistical significance was calculated using the log-rank test. **C** TCGA analysis of *KMT5A* (*SETD8*) relative mRNA expression levels in normal and tumor tissue derived from CRC patients (COAD dataset). **D** Immunohistochemical analysis of SETD8 and $p53^{K382me1}$ on healthy colon mucosa of a healthy subject and on tumor tissue of a $p53^{WT}$ CRC patient. Scale bars, 40 µm. **E** Immunoblot analysis of the indicated total and histone proteins in SY5Y NB cells, HCT116 and LOVO colon cancer cells, and 11 CR-CSphCs (*left panel*). Densitometry analysis of $p53^{K382me1}$ protein levels compared with p53 total protein levels measured as relative density units (RDU) (*right panel*). **F** Immunoblot analysis of the indicated proteins in CRL-1790 and CRL-1831 healthy colon cells, in HCT116 colon cancer cells and in CR-CSphC#8. β-actin was used as loading control. **G** Immunofluorescence analysis of $p53^{K382me1}$ and CD44v6 in tumor tissue derived from a $p53^{WT}$ CRC patient. Nuclei were counterstained by Toto-3. Scale bars, 40 µm. **H** Immunohistochemical analysis of CD44v6 and immunofluorescence analysis of $p53^{K382me1}$ and SETD8 on tumor tissue of two CRC TMAs representative of high staining intensity (#1) or lack of staining (#2), respectively. Nuclei were counterstained by Toto-3. Scale bars, 40 µm. **I** Immunofluorescence analysis of $p53^{K382me1}$ in CRC TMA patients in tumor tissue (*T*) or in the immune cell infiltration (*I*). Four different conditions are indicated (Tum + /Inf-, Tum + /Inf + , Tum-/Inf-, Tum-/Inf +). Nuclei were counterstained by Toto-3. Scale bars, 40 µm. **J** Probability of survival in CRC TMA patients based on the $p53^{K382me1}$ expression in tumor tissue (Tum ±) and/or in the immune cell infiltration (Inf ±). **K** Disease-free survival probability in CRC patients based on $p53^{K382me1}$ expression in tumor tissue or in the immune cell infiltration. See also Tables S1, Table S2, Table S3 and Figure S1

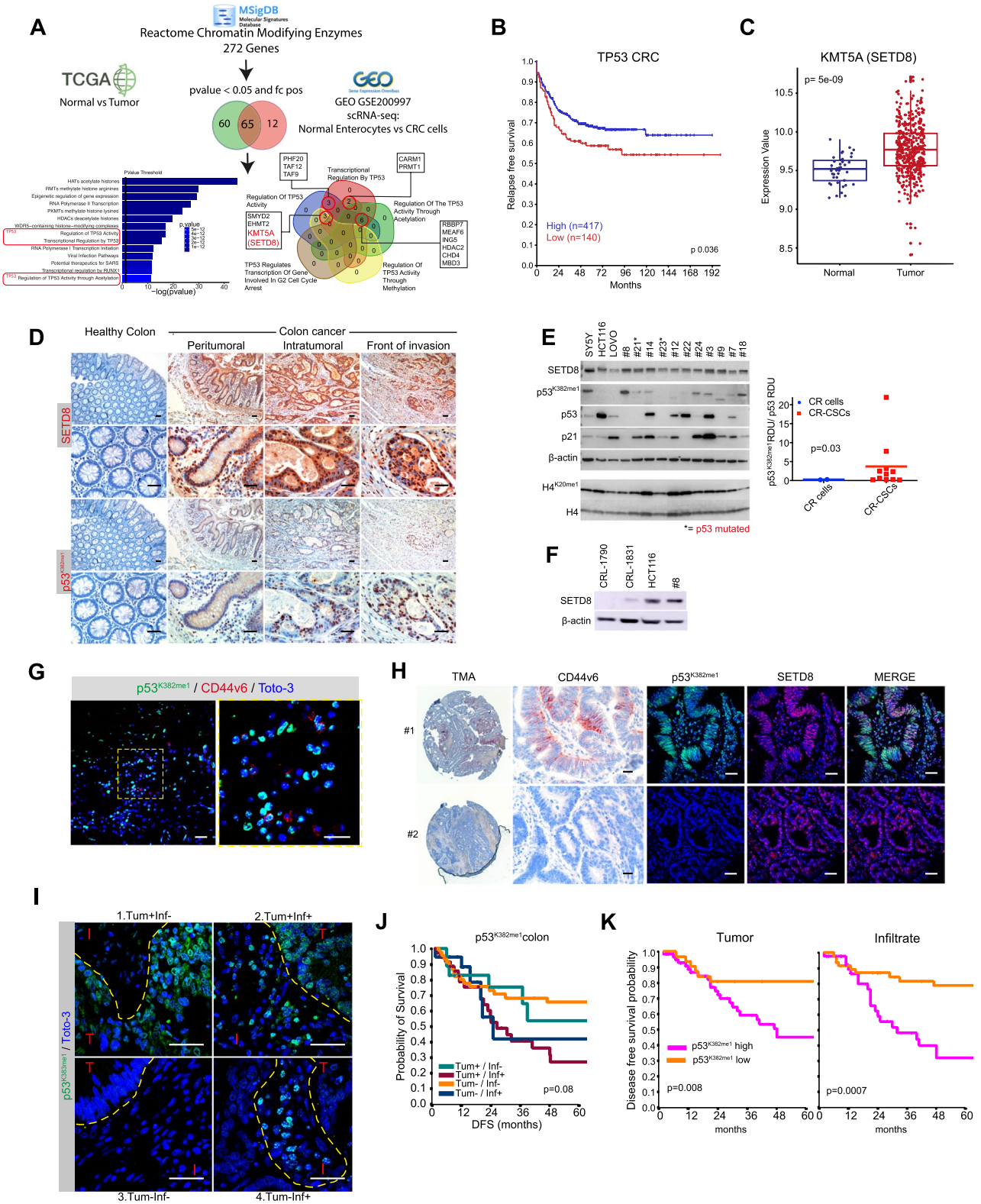

Fig. 1 (See legend on previous page.)

in inflammation, more specifically its role in conversion to pro-tumoral M2 macrophages is complex and poorly explored [19]. To gain insights into the distinct contributions of the epithelial and immune cell compartments to the mechanism of p53 inactivation, we exposed normal colonocytes, CR-CSphCs, and human macrophages to the specified conditioned media (CM) (Fig. 2G). Exclusively, exposure to CM3, which is obtained from the direct interaction between CR-CSphCs and human macrophages (THP1) induced the expression of $p53^{K382me1}$ in all three cell types (Fig. 2G). This phenomenon was paralleled by a down-regulation of p53 target genes, in healthy colon cells, CR-CSphCs and macrophages (Fig. 2H-I; Fig.S2F).

In line with these data, upon CM3 treatment, THP1 cells acquire a TAM M2 phenotype with a higher percentage of cells expressing CD163 and CD206. This effect was reversed by the removal of the CM3 (Fig.S2G). In accordance with the reported data, CM3 exhibited high levels of secreted IL-6 and monocyte-chemoattractant-protein (MCP-1 also known as CCL2) [10] (Fig. 2J; Fig. S2H). A global transcriptomic analysis confirmed that *IL-6* and *MCP-1* levels are significantly overexpressed in patients affected by CRC and IBD compared to healthy subjects (Fig. 2K; Fig.S2I). Exposure of healthy colonocytes, CR-CSphCs, or macrophages to these cytokines, either alone or in combination, led to increased expression levels of $p53^{K382me1}$ and EMT-related genes (Fig. S2J-M). Notably, high expression levels of IL-6 receptor (IL-6R) along with MCP-1 receptor (CD192 also known as CCR2) were observed in CR-CSphC#8 [29] (Fig.S2L).

Moreover, in CR-CSphCs, exposure to CM3 promoted the expression of EMT- and inflammatory response-related genes characterized by the activation of TNFα and IFNα pathways, which was accompanied by a down-regulation of p53 transcriptional activity/signaling pathways and reduced levels of p53 target genes (Fig. 3A-F).

In CR-CSphCs and macrophages, along with the induction of EMT- stemness and Wnt-associated genes such as *AXIN-2* and ß-catenin *(CTNNB1)*, IL-6 or CM3 treatment also led to increased mRNA levels of *SETD8*, *MCP-1* and the enhancer-binding protein transcription factor *(CEBPD)* (Fig.S3A-D). *CEBPD,* also known as C/EBPδ, is a versatile modulator of inflammatory response and differentiation processes, activated by inflammatory factors such as IL-6, TNFα, IFN-γ and LPS with a dual role in cancer [30–32].

Interestingly, ChIP-qPCR analysis revealed that exposure to IL-6 significantly increased the fixation of C/EBPδ to the *SETD8* promoter (Fig. 3G-H; Fig.S3E). These findings indicate that the interplay between CR-CSphCs and macrophages is required for the inactivation of p53 by $p53^{K382me1}$-mediated MCP-1 and IL-6 secretion. This process enhances the transcription of SETD8 through the direct binding of C/EBPδ to the *SETD8* promoter.

Importantly, the increase of SETD8 expression upon CM3 treatment was effectively neutralized through addition of antibodies targeting IL-6 and MCP-1, and downregulation of C/EBPδ (Fig. S3F-G). These data strongly suggest that CR-CSphCs cooperate with TAMs in activating the IL-6/MCP-1/C/EBPδ circuit, which in turn promotes SETD8 transcription. This process is further boosted by the pivotal role of TAMs which

(See figure on next page.)

Fig. 2 $p53^{K382me1}$ expression is specifically enriched in $CD68^+$ macrophages present in IBD and CRC patients. **A** Immunofluorescence analysis of $p53^{K382me1}$ and CD68 in tumor tissue derived from a $p53^{WT}$ CRC patient. Nuclei were counterstained by Toto-3. Scale bars, 40 µm. **B** $p53^{K382me1}$ positivity percentage of $CD68^+$ (macrophages), $CD163^+$ (TAMs), $CD8^+$ (lymphocytes), $CD4^+$ (lymphocytes), $CD15^+$ (B cells) and $CD20^+$ (neutrophils) immune cells in tumor tissues derived from $p53^{WT}$ CRC patients. Data represent mean ± SD of three independent experiments. ns, not significant. **C** Analysis of *KMT5A* (*SETD8*) and *CD68* relative mRNA expression levels in normal and inflamed tissues derived from IBD patients in E-MTAB-184 array express dataset. **D** Immunofluorescence analysis of $p53^{K382me1}$ and CD68 in inflamed and peri-inflamed tissues derived from patients affected by Crohn's disease (CD) and Ulcerative colitis (UC). Nuclei were counterstained by Toto-3. Scale bars, 40 µm. **E** $p53^{K382me1}$ positivity percentage of total cell population (*upper panel*) and $CD68^+$ macrophages (*lower panel*) in IBD patients as in (**D**). Data are expressed as mean ± SD of three independent experiments. **F** Immunohistochemical analysis of $p53^{K382me1}$ on peri-inflamed tissue of a Crohn's disease (CD) patient as measured by Image J software. Scale bars, 40 µm (*left panels*). Scheme showing the basal, transit-amplifying cells (TAC) and apical compartments of a colon crypt (*right upper panel*). $p53^{K382me1}$ positivity percentage of epithelial cells in the indicated colon crypt compartments as shown in the *left panels*. Data are expressed as mean ± SD of three independent experiments. ns, not significant (*right lower panel*). **G** Scheme showing the generation of three conditioned media (CM) and its administration on healthy colon cells, CR-CSphCs and macrophages. Immunoblot analysis showing the expression of the indicated proteins in healthy colon cells, CR-CSphCs#14 and THP1 treated with three CM for 72 h. **H** Heatmap of the p53 pathway-related genes ($2^{-\Delta Ct}$ expression values) in healthy colon cells and CR-CSphCs#14 treated with CM3 for 48 h. Data are presented as normalized mRNA expression values of 2 biological replicates. The color key represents the normalized expression values: blue (low) to red (high). **I** The top 15 differentially expressed canonical pathways in CR-CSphCs#14 treated as in (**H**) obtained by Enrichment Pathway Analysis based on the Reactome Gene set (Molecular Signature Database, MSigDB), utilizing msigdbR library and $p < 0.05$. Pathways related to p53 signaling are among the top differentially expressed pathways. **J** Lollipop plot representing the number of cytokines released by CR-CSphCs#8 and THP1 cells (CM3) compared with CM1 as measured by Luminex Bio-plex assay. Data are expressed as LogFC values of 2 biological replicates. **K** Analysis of *IL-6* and *CCL2* (MCP-1) relative mRNA expression levels in normal and tumor tissues derived from CRC patients in TNM plot dataset. See also Figure S2

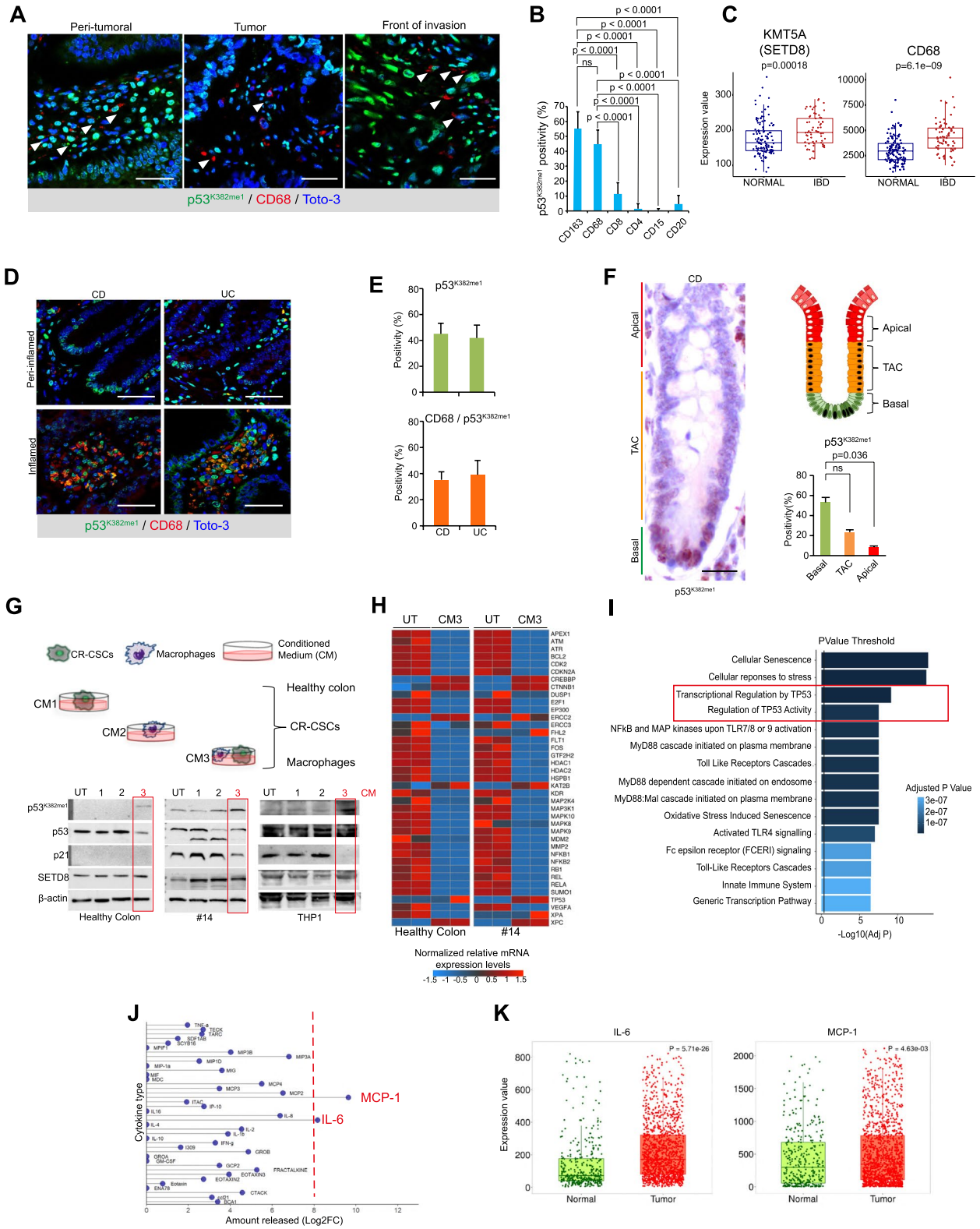

Fig. 2 (See legend on previous page.)

reinforcing the IL-6/MCP-1/C/EBPδ signaling loop enhances cytokine-driven SETD8 expression.

While in THP1 cells SETD8 knockdown significantly reduced IL-6 and MCP-1 secretion, in CR-CSphCs its combination with TP53 knockdown partially restored cytokine secretion (Fig.S3H-L).

These results highlight that SETD8-mediated p53 inhibition enhances IL-6 and MCP-1 secretion by TAMs, and SETD8 targeting restores p53 function reducing pro-inflammatory cytokine secretion levels.

CRC-associated macrophages unveil altered p53 signaling pathway

Given that macrophages could play a role in the driving events leading to the dynamic evolution of the metastatic process or from a chronic inflammatory state to tumor formation, we conducted a detailed examination at the single-cell levels to provide a clearer understanding of the macrophage subpopulation implicated in the mechanism of p53 inactivation by $p53^{K382me1}$. Analysis of a scRNA-seq data (GEO accession number# GSE200997) from 23 CRC patients and their normal counterpart tissues revealed higher expression levels of SETD8 in CR-CSCs (tumor cells cluster2) characterized by high levels of stemness-related markers such as LGR5, CD44 and CD133 and in metaplastic/inflammatory Paneth cells (Fig. 4A-F; Fig.S4A-E). Notably, throughout pseudotime, there was a decrease in *CDKN1A* (p21), while *HDAC2*, the exclusive deacetylase responsible for catalyzing the deacetylation of p53 lysine 382, exhibited an increase from normal to cancer stem cells. This phenomenon was accompanied by higher levels of *MYC*, implying that SETD8 and its non-histone target $p53^{K382me1}$ may also increase during this process (Fig. 4G).

The increased number of tumor-infiltrating macrophages could be further defined into two subpopulations determined by distinct trajectories including $FCN1^+$ pro-inflammatory macrophages and $C1Q^+$ pro-tumoral macrophages (Fig. 5A-B; Fig.S5A-D). Among the $C1Q^+$ macrophages, only the $C1Q^+$ $TPP1^+$ macrophages expressed high levels of CD163, a marker of M2 TAMs, SETD8, p53, HDAC2, IL-6 and MCP1(CCL2) (Fig. 5C-E; Fig.S4E; Fig.S5E-G). $C1Q^+$ $TPP1^+$ macrophages represented the cell subpopulation with the highest expression levels of IL-6 and MCP-1, serving as the main producers of these cytokines within the CRC tumor microenvironment, as determined by their exocytosis potential and secretion scores (Fig.S5H-J; Table S6).

The scRNA-seq transcriptome analysis of $C1Q^+$ $TPP1^+$ macrophages derived from CRC tumor tissues versus normal mucosa showed that the top DEGs analyzed by GSEA and computed with the MSigDB displayed enrichment of genes coupled with the oncogenic signaling pathways, such as MYC and KRAS along with EMT, whereas the inflammatory response was associated with both the $FCN1^+$ and $C1Q^+$ $TPP1^-$ subsets of macrophages (Fig. 5F; H-I). Accordingly, in $C1Q^+$ $TPP1^+$ CRC-infiltrating macrophages, genes related to the p53 signaling pathway were among the top differentially down-regulated, in line with the remarkable presence of $p53^{K382me1}$ in this cell subpopulation (Fig. 5F-G).

These findings suggest that $C1Q^+$ $TPP1^+$ macrophages may represent an M2 TAM pro-tumoral subset bearing high levels of SETD8 and altered p53 signaling, in which

(See figure on next page.)

Fig. 3 Direct interaction between macrophages and CR-CSphCs inhibits p53 transcriptional activity and induces an inflammatory response in CR-CSphCs. **A** Immunoblot analysis showing the expression of the indicated proteins in healthy colon cells and CR-CSphCs (#22 and #14) treated with IL-6 and MCP-1 alone and in combination for 72 h. **B** Heatmap showing the top 189 differentially expressed genes (DEGs) with $Log_2FC \geq 1.5$ and $p < 0.05$ obtained by total transcriptome analysis (RNAseq), in CR-CSphCs#14 treated with CM3 for 48 hr. Data are presented as normalized expression values of 2 biological replicates based on edgeR library analysis. The color key represents the normalized expression values: blue (low) to red (high). **C** The top six differentially expressed canonical pathways in CR-CSphCs#14 treated as in (**B**) defined by Hallmark Gene set based on fgsea library analysis and $p < 0.05$. GSEA (Gene Set Enrichment Analysis) showing the enrichment in TNF alpha signaling via NFKB, EMT and IFN alpha response. **D** Dot plot for the enrichment of p53 signaling pathway-associated genes in CR-CSphCs#14 treated as in (**B**). The color represents p-value and the size indicates the number of genes significantly enriched in the indicated p53 signaling pathways. GeneRatio is calculated as number of enriched genes vs total genes. **E**, **F** P53-related genes differentially regulated in CR-CSphCs#14 treated as in (**B**). Data are presented as Log2FC values of 2 biological replicates. GSEA (Gene Set Enrichment Analysis) showing the reduced enrichment in p53 activity by phosphorylation and p53 transcription of DNA repair genes. **G** ChIP-qPCR for C/EBPδ at the *KMT5A* (SETD8) promoter in THP1 cells untreated and treated with IL-6 for 90 minutes. Data are presented as Fold enrichment of C/EBPδ at the *KMT5A* (SETD8) promoter over IgG control. Data are representative of three independent experiments. Statistical analysis was estimated by two-way ANOVA test. ns, not significant. **H** Schematic model of the proposed mechanism showing the cross-talk between colorectal cancer stem cells (CR-CSCs) and tumor-associated macrophages (TAMs M2). IL-6, secreted by immune cells in the tumor microenvironment, prompts macrophages to secrete MCP-1, which recruits TAMs and facilitates the production of IL-6 by CR-CSCs. In both CR-CSCs and TAMs, an altered IL-6/IL-6R and MCP-1/CCR2 signaling lead to the activation of C/EBPδ, a transcription factor, which directly binds SETD8 promoter resulting in increased SETD8 expression and p53 inactivation through K382 methylation ($p53^{K382me1}$). In CR-CSCs, p53 inhibition enhances stemness and tumorigenic capabilities. See also Figure S3

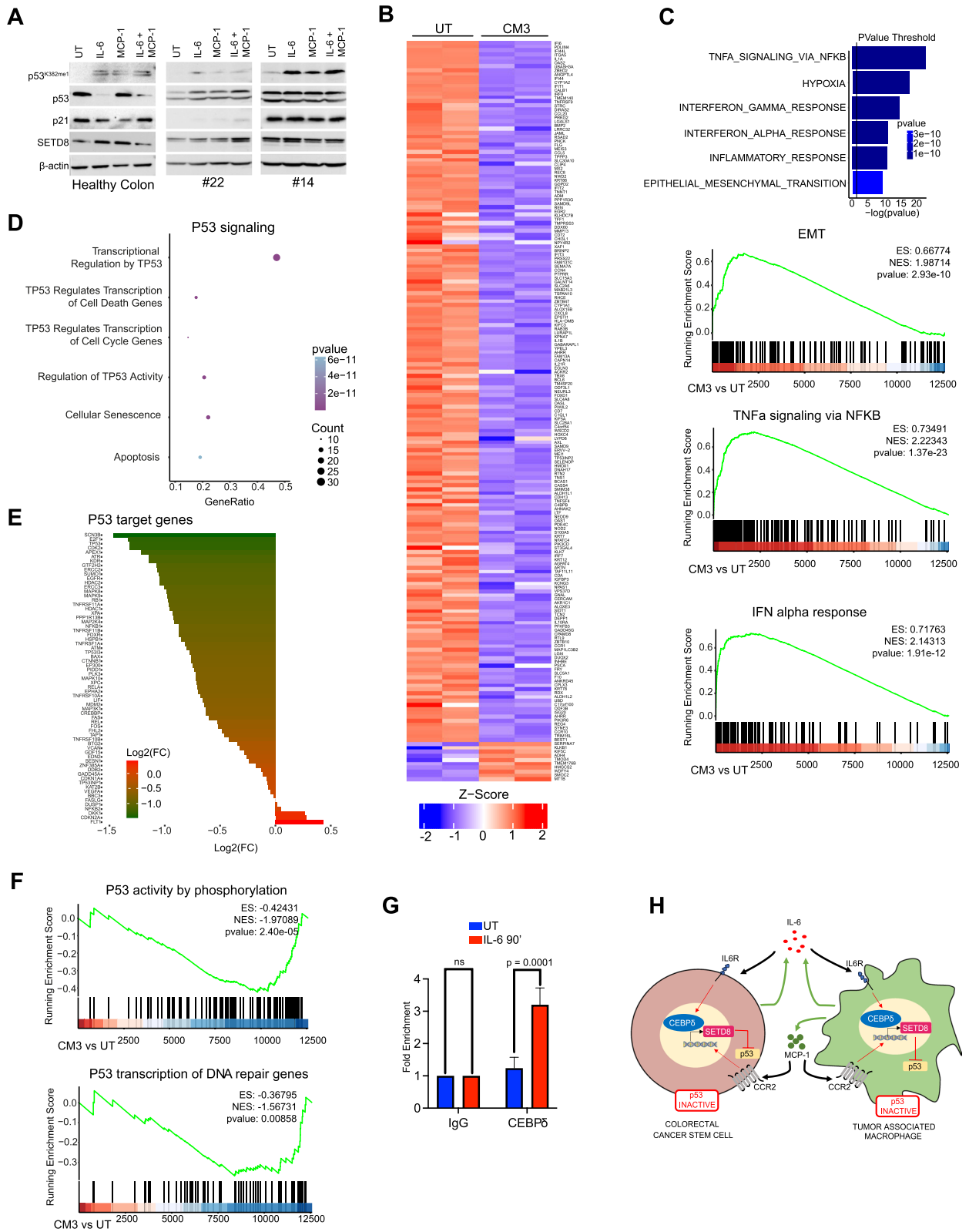

Fig. 3 (See legend on previous page.)

the inactivation of p53 by K382me1 is required. Therefore, the interaction between macrophages and cancer stem cells represents a malevolent alliance that is crucial for understanding tumor biology and developing potential therapeutic strategies.

P53^{K382me1} expression serves as a biomarker for the clinical outcome of CRC patients

In order to understand whether SETD8 is required for the inactivation of p53 and, consequently, could be exploited for preventing or reducing metastasis formation in CRC, we first explored the transition from chronic inflammation to tumor, by conducting a retrospective analysis of p53^{K382me1} expression levels in patients affected by Crohn's disease or ulcerative colitis who later developed CRC. This analysis revealed that the proportion of cells expressing p53^{K382me1}, detected in both immune and epithelial compartments of intestines in patients affected by IBD, increased in the fraction of TPP1^{+}C1Q^{+} macrophages rising from 20 to 60% during the progression to CRC (Fig. 6A-B; Fig.S6A). C1Q, the Complement component 1q which mediates the complement-mediated killing of bacteria in the bloodstream has been described as a key mediator of a neuroimmune interaction that regulates gut motility, supporting its role in physiological and pathological processes [33]. Analysis of different cohorts of CRCs showed a significative negative correlation between the expression of CD68 and CD163 and the relapse-free survival of CRC patients (Fig. 6C; Fig.S6B-C). Consistent with these findings, immunohistochemical analysis of inactive p53 in tissue sections of tumor specimens obtained from advanced CRCs, highlighted that expression p53^{K382me1} co-localized with macrophages expressing TPP1 and C1Q, which were predominantly located at the front of tumor invasion (Fig. 6D-G). Notably, the receptor for C1Q, C1QR, is highly expressed on CR-CSphCs, indicating an additional potential mechanism of interaction between CR-CSphCs and C1Q^{+} macrophages (Fig. 6H).

In accordance with the immunohistochemical data, the analysis of different cohorts of CRC patients showed a significative negative correlation between the expression of C1Q and C1QR and the relapse-free survival of CRC patients, and correlated the detection of C1Q and TPP1, or C1Q and C1QR, with worse overall survival (Fig. 6I-J; Fig.S6D-E).

Targeting SETD8/p53^{K382me1} axis impairs tumor growth and metastasis formation

To explore the potential of targeting SETD8 pathway to impede the tumorigenic and metastatic capabilities in CRC, we examined the impact of genetically inhibiting SETD8 in subcutaneous, orthotopic and intra-splenic preclinical models, assessing both CR-CSphCs and macrophages for their dependence on SETD8. Orthotopic injection of CR-CSphCs, transduced with lentiviral vector (pTRIPZ) encoding for specific SETD8 small hairpin RNA (shRNA) sequences, led to a reduction in p53^{K382me1}, SOX-2, CD133 and NANOG protein levels, while significantly decreasing cell migration without compromising cell growth (Fig.S6F-I). Accordingly, the tumorigenic and metastatic potential of orthotopically and subcutaneously injected CR-CSphCs was delayed by doxycycline-induced shSETD8 expression and restored after doxycycline treatment suspension (Fig. 7A-B; Fig.S6J-K). In addition to reduced p53^{K382me1} and SETD8 levels, harvested tumor metastatic lesions treated with shSETD8, showed fewer cells expressing CK20 compared with those treated with empty vector (pTRIPZ) (Fig. 7C; Fig.S6L-M). To determine whether SETD8 expression in macrophages cooperates with SETD8 expression in CR-CSphCs to promote tumor progression, we co-injected THP1 cells, transduced with shSETD8, with shSETD8-CR-CSphCs subcutaneously and into mouse spleen, mimicking a pre-clinical metastatic CRC model. SETD8 knockdown in macrophages and CR-CSphCs abrogated tumor metastasis outgrowth prolonging the survival rate and indicating that SETD8 is required in both cell subtypes for tumor growth and predominantly in CR-CSphCs for tumor spreading (Fig. 7D-I; Fig.S6N). In line with these data, TP53 knockdown in combination with SETD8 genetic inhibition in CR-CSphCs, restored xenograft tumor volume shortening survival of mice when

(See figure on next page.)

Fig. 4 scRNA-seq data analysis reveals high expression levels of SETD8 in CR-CSCs and Paneth cells. **A**, **B** UMAP visualization of major populations in normal colon mucosa (**A**) and tumor tissue of CRC patients (**B**). **C** UMAP visualization of the epithelial compartment in CRC (Bulk tumor cells=Tumor cells 1; Cancer stem cells=Tumor cells 2). **D** Trajectory analysis of the epithelial compartment in CRC. Black circles indicate the start or end point of the trajectory. The red arrow indicates normal stem cells. The red circle indicates metaplastic or inflammatory Paneth cells. The blue circle indicates Cancer stem cells. **E** UMAP visualization of the epithelial compartment in CRC colored by *KMT5A* (SETD8) expression. **F** Dot plot for the expression of *KMT5A* (SETD8) and *TP53* genes in all the subpopulations of the epithelial compartment in CRC. The color represents the scaled average expression of *KMT5A* and *TP53* genes in each cell type, and the size indicates the proportion of cells expressing *KMT5A* and *TP53* genes. **G** Expression of *MYC*, *CDKN1A* and *HDAC2* as a function of pseudotime in the epithelial compartment in CRC, with cells colored according to the corresponding cell type. See also Figure S4

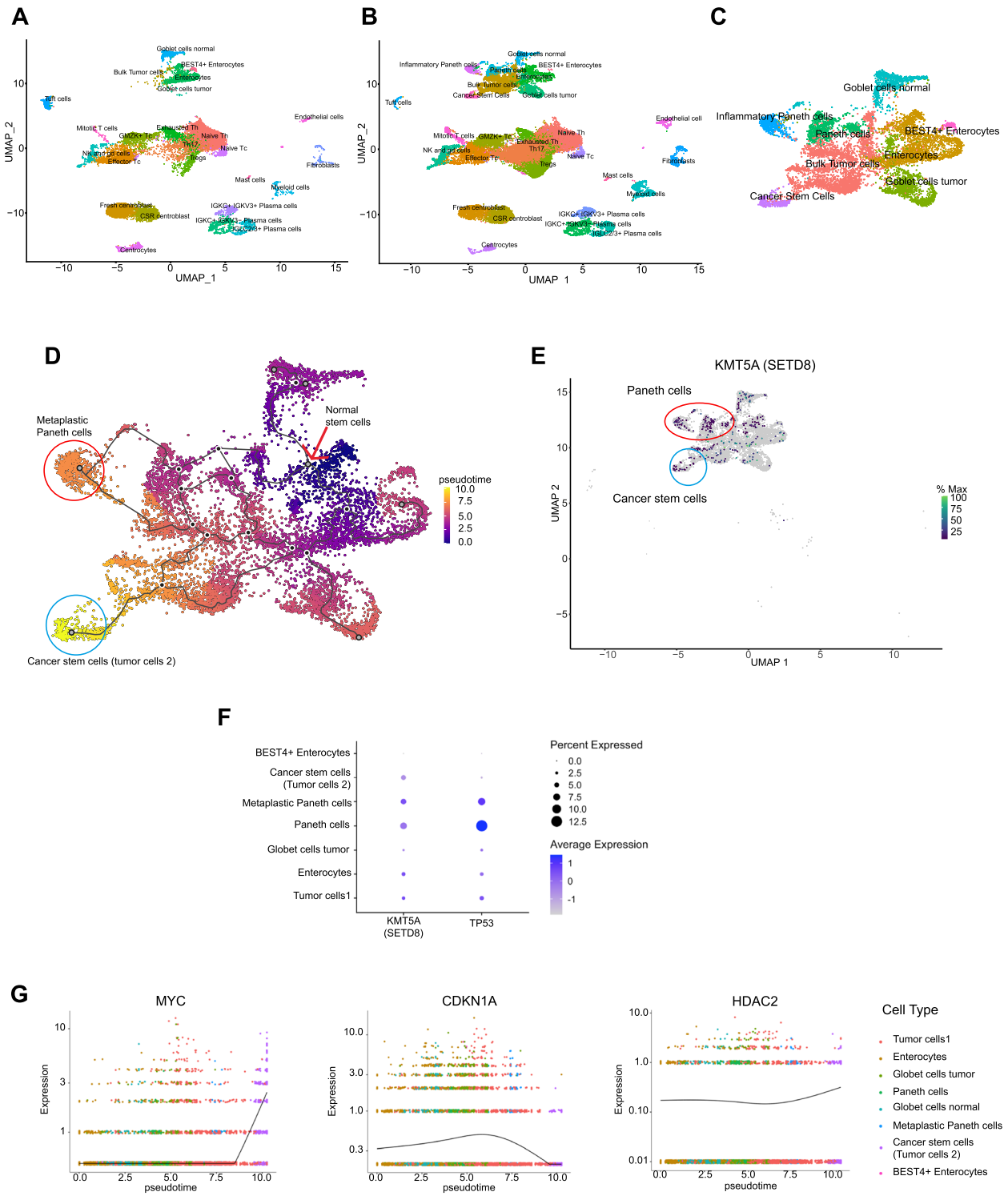

Fig. 4 (See legend on previous page.)

subcutaneously co-injected with THP1 cells (Fig. 7D; F). These findings indicate that, in CRC the pro-tumorigenic role of SETD8 relies on p53.

To further investigate the therapeutic potential of SETD8 inhibition, CR-CSphCs, expressing high levels of SETD8, were treated with a selective substrate-competitive inhibitor of SETD8, the small molecule UNC0379 [34]. Regardless of the p53 mutational background, this treatment, led to a marked reduction in the number of CR-CSphCs, likely by increasing apoptotic events and growth arrest, as evidenced by heightened expression levels of pro-apoptotic genes, and an increase in G0-G1 phase, coupled with a reduction in both S- and G2/M phases of the cell cycle (Fig. 8A; Fig.S7A-G). In line with a more pronounced cell death, $p53^{K382me1}$ and $H4^{K20me1}$ protein levels gradually decreased with increasing UNC0379 dose concentration, paralleled by a restoration of p53 and p21 levels and a reduction of colony-forming capability of CSphCs (Fig. 8B; Fig.S7H). UNC0379 treatment of tumor xenografts, generated by the subcutaneous injection of CR-CSphCs alone or in combination with THP1 cells, delayed the disease progression and prolonged the survival probability (Fig. 8C; Fig.S7I-K). In tumor xenografts, generated by the subcutaneous co-injection of CR-CSphCs and THP1 cells, these effects were significantly enhanced when UNC0379 treatment was combined with Tocilizumab, an IL-6 receptor inhibitor (Fig. 8C-E; Fig.S7L-M). TP53 knockdown significantly reduced the benefits of SETD8 inhibition by UNC0379, even in combination with Tocilizumab, leading to restored tumor growth (Fig. 8C). These findings underscore the critical role of the SETD8/$p53^{K382me1}$ axis in CRC progression and its potential as a therapeutic target.

Transcriptomic analysis of CR-CSphCs exposed to both genetic and pharmacological SETD8 inhibition identified 21 downregulated genes that were enriched for gene ontology (GO) categories related to the activation of cell proliferation and migration mechanisms (Fig.S8A-E).

In summary, the findings from this study have pinpointed a distinct subset of $C1Q^+$ and $TPP1^+$ macrophages that undergo p53 inactivation through the SETD8/$p53^{K382me1}$ axis. This subset potentially represents a shared mechanism involving direct communication between intestinal stem cells and cancer stem cells (CSCs), along with the induction of SETD8 gene transcriptional regulation mediated by IL-6 and CCL2 during intestinal chronic inflammation and progression to cancer (Fig. 8F).

Discussion

Here, we demonstrated that CR-CSCs and tumor-associated macrophages, mainly located at the invasive tumor front, express high levels of SETD8, a histone methyltransferase that functionally inactivates p53 through the production of $p53^{K382me1}$. SETD8 and other epigenetic remodelers like LSD1, known to suppress p53 activity, have been linked to sustaining the self-renewal, migration, and invasion capabilities of CR-CSCs, by activating the Wnt pathway [25, 35, 36]. SETD8 promotes stem-like properties, EMT and migratory capabilities in pancreatic, gastric and lung cancers [37–39]. Genetic or pharmacological inhibition of SETD8 reduces stemness markers, EMT-associated genes and colony-forming capability of CR-CSphCs, underlying the contribution of SETD8 to the metastatic potential of CR-CSCs, as evidenced by high expression levels of p53 functionally inactivated, $p53^{K382me1}$, in approximately 70% of CD44v6-positive cells observed predominantly at the invasive tumor front of the analyzed CRC tissues. CD44v6 is a functional marker that demarcates CR-CSCs able to migrate and develop CRC metastasis [26]. While p53 inactivation boosts the stemness properties of cancer cells, its activation abolishes the self-renewal properties of leukemia stem cells that persist in patients affected by chronic myeloid leukemia as residual disease [17, 40, 41]. About 75% of our CR-CSphCs

(See figure on next page.)

Fig. 5 scRNA-seq data analysis identifies $C1Q^+$ $TPP1^+$ macrophages as TAM M2 with an altered p53 signaling in CRC. **A** UMAP visualization of macrophage subpopulations in normal colon mucosa and tumor tissue of CRC patients. **B** Trajectory analysis of macrophage subpopulations in CRC. FCN1 trajectory and C1Q trajectory show opposite directions. **C**, **D** and **E** Dot plot for the expression of *CD163*, *KMT5A* (SETD8), *TP53, CDKN1A, IL6* and *CCL2* (MCP-1) genes in the indicated macrophage subpopulations in CRC. The color represents the scaled average expression of the indicated genes in each cell type, and the size represents the proportion of cells expressing the indicated genes. **F** Dot plot for the enrichment of the indicated signaling pathway-associated genes expressed as normalized enrichment score (NES), in $C1Q^+$ $TPP1^+$ macrophages in CRC tissue vs normal mucosa. The color represents p-value and the size indicates the number of genes significantly enriched in the indicated pathways. P53 pathway is among the top down-regulated pathways. **G** Immunofluorescence analysis of TPP1, C1Q, FCN1 and $p53^{K382me1}$ in tumor tissue derived from a $p53^{WT}$ CRC patient. The yellow square indicates the inset shown on the right. Scale bars, 20 µm (*left panels*). $p53^{K382me1}$ positivity percentage of $TPP1^+$/$C1Q^+$ and $FCN1^+$ macrophages, in the indicated compartments of tumor tissue derived from a $p53^{WT}$ CRC patient as shown in *left panels*. Data are expressed as mean ± SD of three independent experiments. ns, not significant (*right panels*). (H, I) Dot plot for the enrichment of the indicated signaling pathway-associated genes expressed as normalized enrichment score (NES), in $C1Q^+$ $TPP1^-$ macrophages (**H**) and in $FCN1^+$ macrophages (**I**) in CRC tissue vs normal mucosa. The color represents *p*-value and the size indicates the number of genes significantly enriched in the indicated pathways. See also Figure S5 and Table S5, Table S6

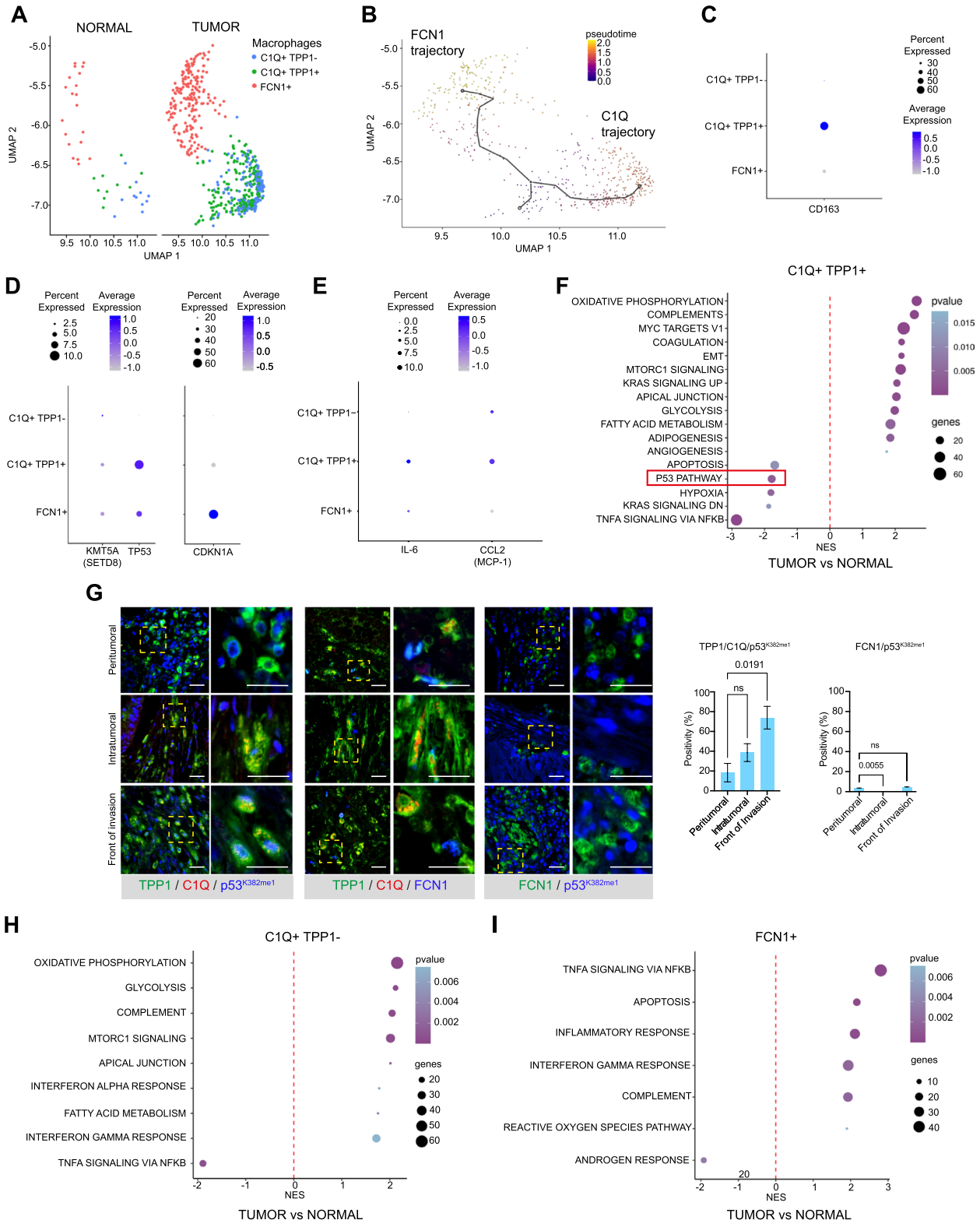

Fig. 5 (See legend on previous page.)

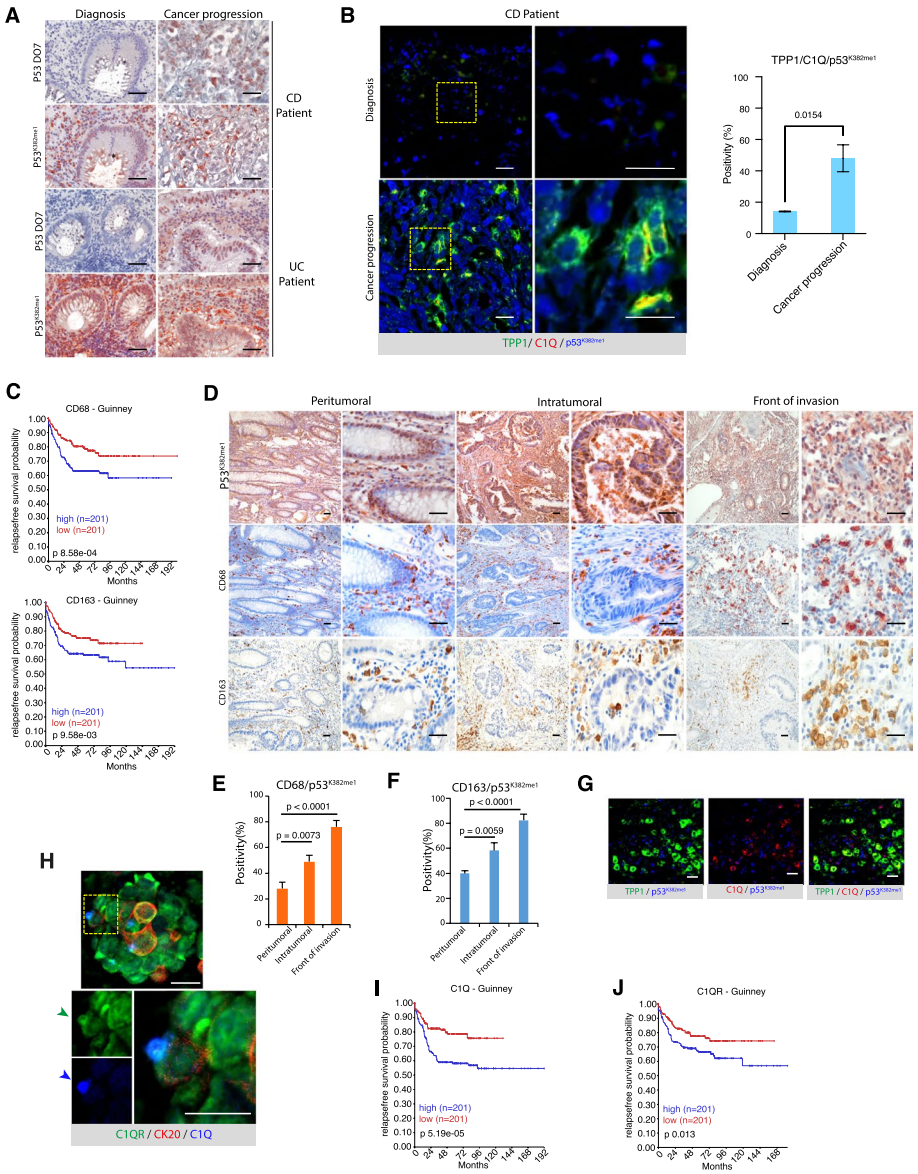

Fig. 6 In IBD and CRC patients with CMS4, SETD8 is correlated with poor prognosis and p53 is methylated on lysine 382 in C1Q^{+}TPP1^{+} macrophages. **A** Immunohistochemical analysis of p53 DO7 and p53^{K382me1} on colon mucosa of a Crohn's disease (CD) patient and an Ulcerative colitis (UC) patient at diagnosis and CRC progression. Scale bars, 40 µm. **B** Immunofluorescence analysis of TPP1, C1Q and p53^{K382me1} on colon mucosa of a Crohn's disease (CD) patient at diagnosis and at CRC progression. Scale bars, 20 µm (*left panels*). p53^{K382me1} positivity percentage of TPP1^{+}/C1Q^{+}macrophages in colon mucosa of a Crohn's disease (CD) patient at diagnosis and at CRC progression as shown in *left panels*. Data are expressed as mean± SD of three independent experiments (*right panel*). **C** Relapse-free survival (RFS) analysis of CD68 and CD163 expression in CRC patients from R2 database (Guinney dataset). Statistical significance was calculated using the log-rank test. **D** Immunohistochemical analysis of p53^{K382me1} , CD68 and CD163 on tumor tissue derived from a p53^{WT} CRC patient with consensus molecular subtype 4 (CMS4). Scale bars, 40 µm. (E, F) p53^{K382me1} positivity percentage of CD68^{+} macrophages (**E**) or CD163^{+} macrophages (**F**) in peritumoral, intratumoral tissues and invasive front derived from a p53^{WT} CRC patient with CMS4 as shown in (**D**). **G** Immunofluorescence analysis of TPP1, C1Q and p53^{K382me1} on tumor tissue derived from a p53^{WT} CRC patient with CMS4. Scale bars, 20 µm. **H** Immunofluorescence analysis of C1QR, CK20 and C1Q in CR-CSphC#8 and THP1 cells. Scale bars, 20 µm. **I**, **J** Relapse-free survival (RFS) analysis of C1Q and C1QR expression in CRC patients from R2 database (Guinney dataset). Statistical significance was calculated using the log-rank test. See also Figure S6

collection display high levels of p53^{K382me1}. Targeting the SETD8/p53^{K382me1} axis in CR-CSCs reduces stem-like features and EMT phenotype, leading to decreased cell proliferation and enhanced apoptosis through the activation of p53 transcriptional activity, posing it as a promising therapeutic strategy in advanced and metastatic CRC

patients. p53 dysfunction within tumors boosts chronic inflammation, thereby advancing tumor development. This process influences the immune response by causing abnormal recruitment of T and myeloid cells, ultimately facilitating immune evasion [42]. In tumor tissues obtained from colorectal cancer (CRC) patients, expression of $p53^{K382me1}$ was not only confined to CR-CSCs endowed with high metastatic potential but was also evident in approximately 80% of $CD68^+$ tumor-associated macrophages (TAMs) of the M2 phenotype, while no detectable expression was noted in $CD4^+$, $CD8^+$ T cells or $CD15^+$ neutrophils or $CD20^+$ B cell populations. Although the mechanisms underlying p53 inactivation in macrophages remain largely unexplored, these findings likely result from the pivotal role of p53 in governing macrophage differentiation, hindering their polarization towards the M2 phenotype [18, 19]. Additionally, a functional p53 status in macrophages likely plays a protective role in inflammatory settings, limiting the initiation and invasion of colorectal cancer [21]. Macrophages, particularly those associated with tumors (TAMs), play a significant role in promoting the development and spread of various types of tumors, by inducing an enrichment of CSCs and their stem-like properties, largely through the modification of cytokine production [43–46]. Patients with IBD who later develop CRC exhibit an increased presence of macrophages expressing high levels of $p53^{K382me1}$ compared to IBD patients at the time of diagnosis. This expression is observed in the intestinal stem compartment and inflammatory Paneth cells, at the basal level of partially conserved colon crypts, and gradually decreases along the transit-amplifying cell zone and apical area. This phenomenon is significant as it suggests a potential link between the presence of these macrophages and the transition from IBD to CRC, whose association is further supported by the plasticity of Paneth cells, which are considered the cells of origin of CRC in an inflammatory state [47].

The analysis of pseudotime trajectory reveals that normal intestinal cells, during their transition to CSCs, acquire higher levels of MYC and HDAC2, the sole deacetylase responsible for catalyzing the deacetylation of lysine 382, while displaying decreased levels of CDKN1A (p21). Accordingly, HDAC2 expression is particularly enriched in CSCs, Paneth cells and $C1Q^+$ $TPP1^+$ macrophages. These findings support the involvement of p53 inactivation, mediated by K382me1, in this process.

The interaction between CR-CSCs and macrophages is essential for CRC tumorigenesis and metastasis [48–51]. The interaction also leads to the inactivation of p53 by $p53^{K382me1}$ through the secretion of IL-6 and MCP-1, which enhances the transcription of SETD8 via the direct binding of C/EBPδ to the SETD8 promoter. Consequently, under chronic inflammatory stimuli, altered cytokine production through the IL-6/MCP-1/C/EBPδ circuit induces high expression levels of SETD8 and subsequently $p53^{K382me1}$ in both cell compartments, CR-CSCs and macrophages, by the

(See figure on next page.)

Fig. 7 SETD8 genetic inhibition in CSCs and macrophages impairs tumor growth, metastasis formation and prolongs murine survival in in vivo models of CRC. **A**, **B** In vivo whole-body imaging analysis (**A**) and kinetics of tumor formation (**B**) detected by in vivo imaging analysis at the indicated time following orthotopic injection of CR-CSphC#8 stably transduced with doxycycline (DOXY)-inducible vectors pTRIPZ and shSETD8. Time −2 weeks indicates the day of cell implantation. After 2 weeks, DOXY was added to both groups of mice (pTRIPZ and shSETD8). Bars show the tumor size average of 6 mice/group ± SEM. Slopes of the growth rate were compared by Mann–Whitney test. **C** Immunohistochemical analysis of SETD8, $p53^{K382me1}$ and CK20 on 2 tumors randomly chosen from each group divided as in (**B**) collected 4 weeks after the injection and 2 weeks after doxy treatment. Scale bars, 40 µm. **D** Xenograft tumor size in mice subcutaneously co-injected with CR-CSphC#8 and THP1 cells. CR-CSphC#8 and THP1 cells were both stably transduced with doxycycline (DOXY)-inducible vectors pTRIPZ and shSETD8 alone or in combination with shTP53. Day 0 indicates the day of cell implantation. Doxycycline (DOXY) was added after tumors reached 75-100 mm^3, 12 days after the injection. Bars show the tumor size average of 6 mice/group ± SEM. Slopes of the growth rate were compared by t-test. **E** Immunohistochemical analysis of CK20 and CD68 on a tumor generated from the subcutaneous co-injection of CR-CSphC#8 and THP1 cells stably transduced with doxycycline (DOXY)-inducible vector pTRIPZ. Scale bars, 40 µm. **F** Kaplan-Meier graphs showing the murine survival upon SETD8 silencing alone or in combination with shTP53 in mice treated as in (**D**). The statistical significance between two treatment groups was evaluated using a log rank test. **G** Kinetics of metastasis formation detected by in vivo imaging analysis at the indicated time following spleen injection of CR-CSphC#8 stably transduced with doxycycline (DOXY)-inducible vectors pTRIPZ and shSETD8. Data are expressed as mean ± SD of 6 mice analyzed. Slopes of the growth rate were compared by t-test. **H** In vivo whole-body imaging analysis of mice treated as in (**G**) and analyzed at the indicated time points after splenectomy. **I** Photons count of all metastatic sites (intestine, lung and liver) in mice following spleen injection of CR-CSphC#8 and THP1 cells both stably transduced with doxycycline (DOXY)-inducible vectors pTRIPZ and shSETD8. Data are expressed as mean ± SD of 6 mice analyzed. The statistical significance between the treatment groups was evaluated using a t-test (*upper panel*). Representative in vivo imaging analysis of metastatic foci in the intestine, lung and liver of mice treated as indicated (*lower panels*). See also Figures S6 and S7

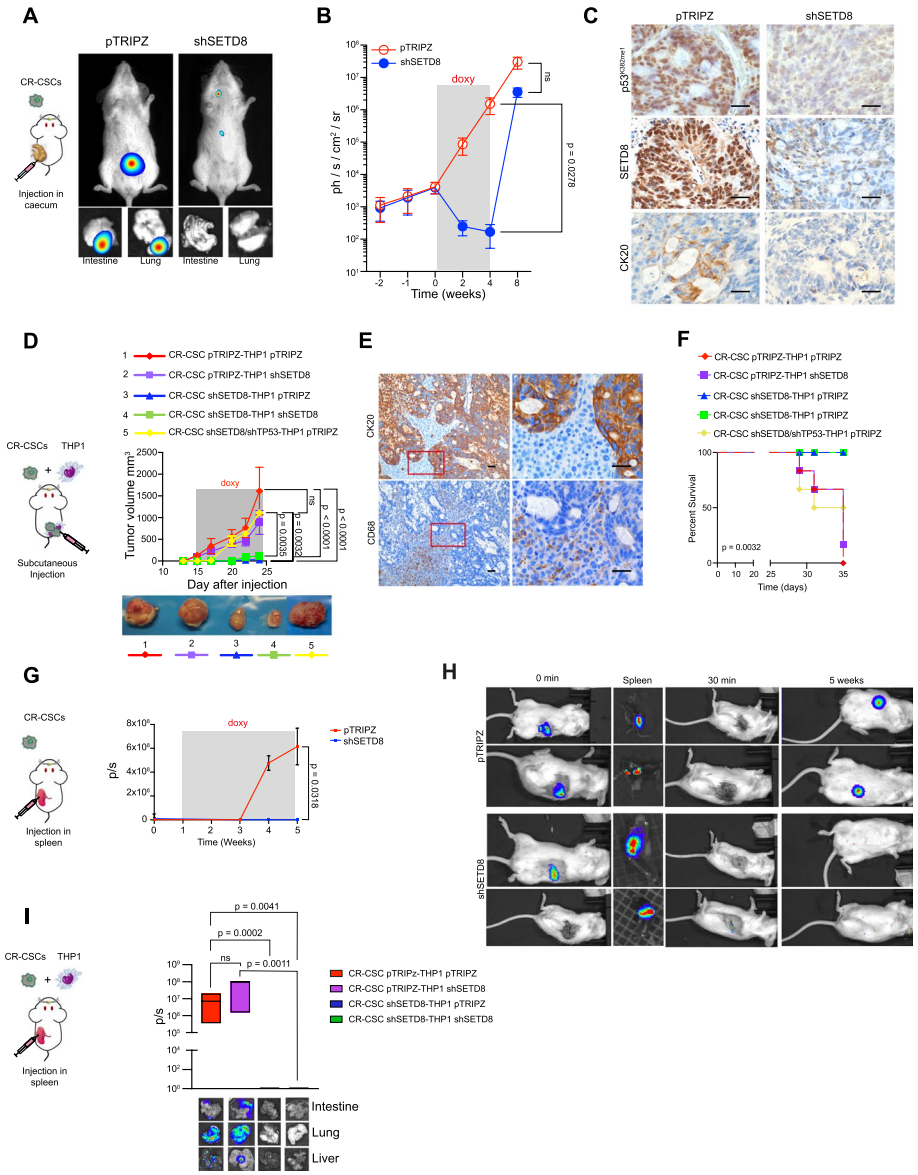

Fig. 7 (See legend on previous page.)

transcriptional inactivation of p53 target genes and the enhanced expression of genes associated with EMT and inflammatory responses.

Given the mutual dependency of IL-6 and MCP-1, IL-6 prompts macrophages to secrete MCP-1, which subsequently stimulates IL-6 release from human epithelial cells [52]. The strong induction of MCP-1 production by IL-6, likely, leads to the recruitment of TAMs and facilitates the production of IL-6 by CR-CSCs. This, in turn, induces the transcription of C/EBPδ, forming a complex regulatory feedback loop, suggesting that macrophages undergo epigenetic reprogramming, mediated by SETD8, upon chronic inflammatory stimuli. The subset of $C1Q^{+}$ $TPP1^{+}$ macrophages represents the M2 TAM pro-tumoral subset characterized by high levels of SETD8, CD163, HDAC2, IL-6, and MCP-1 and associated with increased expression of KRAS, MYC and EMT-related genes. Conversely, the transcriptomic profile of the pro-inflammatory $FCN1^{+}$ and $C1Q^{+}$ $TPP1^{-}$ macrophage subsets is enriched in genes related to the inflammatory response. The complement component 1q (C1Q) is known for its role in the complement system,

which is crucial for non-specific immune functions and the first line of defense against pathogens [33]. Recent evidence has highlighted the involvement of C1Q/C1QR axis in promoting tumor infiltration and cancer metastasis, labeling an aggressive leukemia stem cell population [53–55]. The interaction between the specialized macrophage subset $C1Q^+$ and C1QR-expressing CR-CSCs seems to play a significant role in promoting CRC, providing evidence for a clinical impact and opportunities for selectively targeting the cross-talk between macrophages and tumor cells [56].

$C1Q^+$ $TPP1^+$ macrophages and neutrophils are the primary sources of IL-6 and MCP-1 in CRC tumor microenvironment. While $C1Q^+$ $TPP1^+$ macrophages display high levels of SETD8 expression and impaired p53 signaling, neutrophils do not share these features. This distinction highlights the unique role of macrophages in CRC progression. Unlike resident macrophages, neutrophils are peripheral cells that contribute to chronic inflammation and tumorigenesis but are not involved as target cells in the IL-6/MCP-1/C/EBPδ circuit responsible for driving SETD8 upregulation. This conclusion is further supported by the fact that neutrophils exhibit low levels of SETD8 expression and almost undetectable $p53^{K382me1}$ levels, underlying their limited role in this specific pathway.

Several approaches have been described to target p53 by restoring its function, with many ongoing clinical trials, mainly in leukemias but also in solid tumors, including CRC (NCT03555149), with low side effects already registered [57].

UNC0379, the SETD8 substrate competitive inhibitor [34], treatment in combination with Tocilizumab, an anti-IL-6 receptor (NCT05769959, NCT03866239, NCT04291755) enhanced anti-tumor and -metastatic effects in CRC mouse avatars. These findings suggest a promising therapeutic strategy to activate p53 by inhibiting SETD8 in advanced CRC patients, particularly in inflammation-induced CRCs. In this context, $p53^{K382me1}$ emerges as a critical biomarker of adverse prognosis, demarcating both CR-CSCs with high metastatic potential and $C1Q^+$ $TPP1^+$ pro-tumoral TAMs M2, which are critically involved in the main features of inflammation-induced CRC progression.

Conclusions

Mechanisms of p53 inactivation in colorectal cancer (CRC) cells and tumor-associated macrophages (TAM) are not fully understood. Here, we demonstrate that p53 is inactivated by SETD8-mediated methylation on lysine 382 ($p53^{K382me1}$) in colorectal cancer stem cells (CR-CSCs) and in $C1Q^+$ $TPP1^+$ macrophages (TAM M2). SETD8-mediated p53 inactivation in CR-CSCs promotes their stemness and invasive capabilities while in macrophages it predicts their conversion to the pro-tumorigenic M2 phenotype, thus contributing to CRC progression. An altered secretion of IL-6 and MCP-1 with increased levels of the transcription factor CEBPD, leads to enhanced SETD8 transcription and p53 inactivation. Of note, $p53^{K382me1}$ serves as an independent prognostic factor in patients with CRC. Targeting SETD8/$p53^{K382me1}$ axis using the SETD8 inhibitor UNC0379 in combination with the anti-IL-6 receptor antibody Tocilizumab, impairs tumor growth

(See figure on next page.)

Fig. 8 UNC0379, SETD8 inhibitor, impairs CSC proliferation reducing $p53^{K382me1}$ levels and enhances the anti-tumor effects of Tocilizumab in in vivo CRC models. **A** Cell viability percentage of CRL-1831 and CR-CSphCs#8, #3, #22, #24, #18 and #14 treated with SETD8 inhibitor, UNC0379, at the indicated time and concentrations. Data are presented as percentage of cell number over control ± SD of three independent experiments. Images showing CR-CSC#8 treated with UNC0379 at the indicated concentrations for 72 h. Scale bars, 20 µm (*right panels*). **B** Immunoblot analysis of the indicated proteins in CR-CSphCs#8 and #24 treated with UNC0379 at the indicated concentrations. Densitometric analysis of $p53^{K382me1}$ levels normalized to p53 protein levels and of $H4^{K20me1}$ levels normalized to H4 protein levels upon UNC0379 treatment for 48 hr calculated as RDU using ImageJ software. **C** Xenograft tumor size in mice subcutaneously co-injected with THP1 cells and CR-CSphC#8 transduced with control vector (pTRIPZ) or with shTP53, upon treatment with UNC0379 or Tocilizumab alone or in combination. Day 0 indicates the day of cell implantation. Treatment was added after tumors reached 75-100 mm^3, 12 days after the injection. Bars show the tumor size average of 6 mice/group ± SEM. Slopes of the growth rate were compared by t-test. **D** Immunohistochemical analysis of SETD8 and $p53^{K382me1}$ on tumors generated from the subcutaneous co-injection of CR-CSphC#8 and THP1 cells treated with UNC0379 or Tocilizumab alone or in combination. Scale bars, 40 µm. **E** Immunofluorescence analysis of CD68 and $p53^{K382me1}$ on tumors generated from the subcutaneous co-injection of CR-CSphC#8 and THP1 cells treated as in (**C**). Nuclei were counterstained by Toto-3. Scale bars, 20 µm. **F** Model of $p53^{K382me1}$ expression during chronic inflammation and CRC progression. Upon chronic inflammatory stimuli, p53 is inactivated in both macrophages and intestinal stem cells by methylation on lysine 382 ($p53^{K382me1}$) mediated by SETD8. During progression to CRC, tumor-promoting macrophages TAM M2 expressing C1Q/TPP1 can activate CR-CSC functions by an altered cytokine secretion, particularly IL-6 and MCP-1, contributing to the elevated levels of SETD8 and p53 inactivation by $p53^{K382me1}$. Finally, the migrating CSCs $CD44v6^+$ can invade the metastatic site and repopulate a lineage of progenitors (TAC) and differentiated cells (TDC) with an inactive p53. A combinatorial treatment of SETD8 inhibitor (UNC0379) and IL-6R inhibitor (Tocilizumab) may impair tumor growth by counteracting SETD8/$p53^{K382me1}$ axis and IL-6 signaling in both CR-CSphCs and TAM M2 *(Mj: macrophage; ISC: intestinal stem cell; TAM: tumor-associated macrophage; CR-CSC: colorectal cancer stem cell; TAC: transit amplified cell; TDC: tumor differentiated cell)*. See also Figures S7 and S8

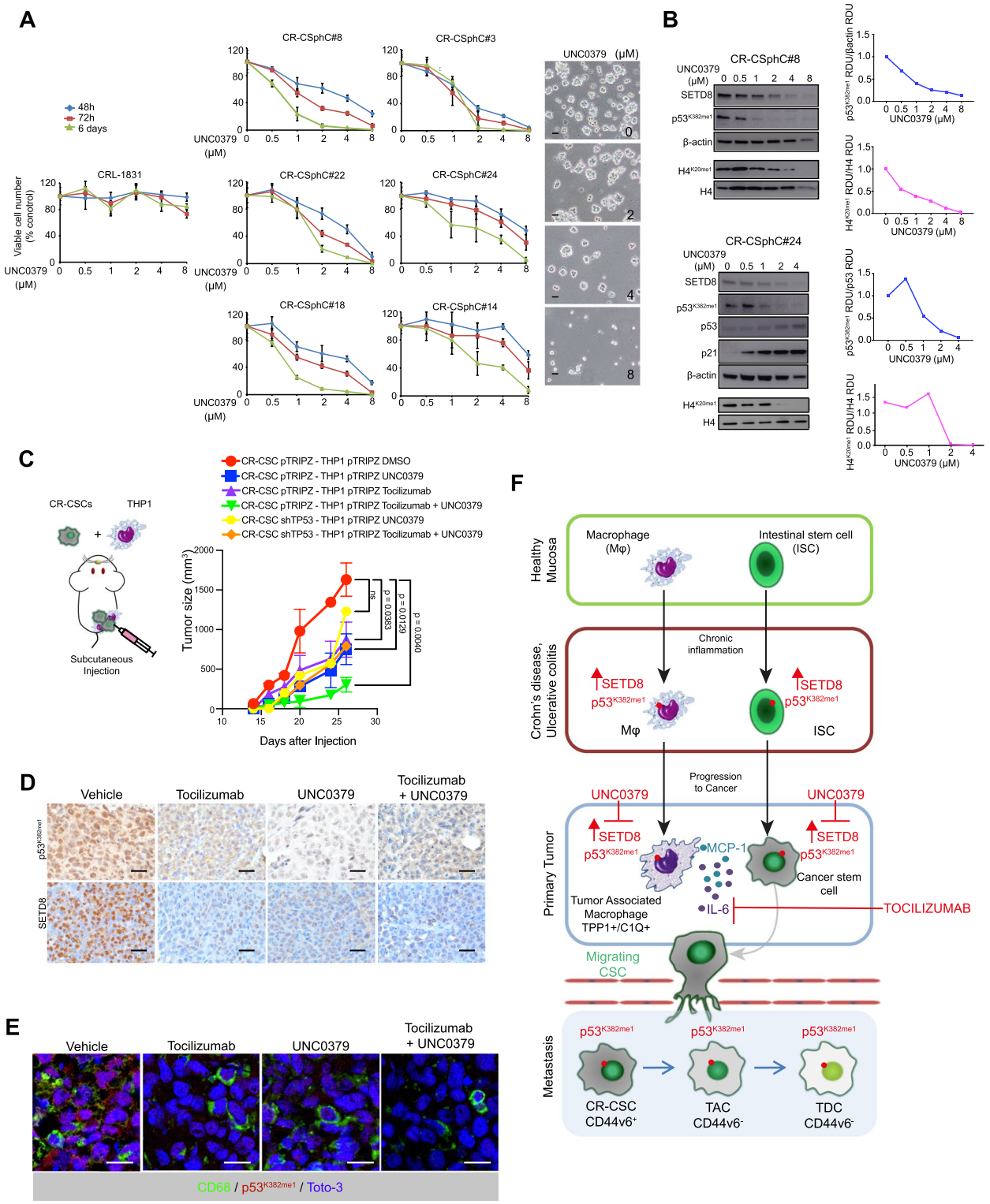

Fig. 8 (See legend on previous page.)

and metastasis formation in CRC mouse models. These findings indicate that the inactivation of p53 by p53^{K382me1} may be an early step in tumor initiation particularly in inflammation-induced CRC, and that targeting SETD8/p53^{K382me1} in both tumor cells and immune cell infiltration represents a promising strategy for treating advanced CRC.

Abbreviations

CRC	Colorectal cancer
IBD	Inflammatory bowel disease
CR-CSC	Colorectal cancer stem cell
CR-CSphC	Colorectal cancer sphere cell
TAM	Tumor-associated macrophage
C1Q	Complement component 1q
C1QR	Complement component 1q receptor
H&E	Hematoxylin and eosin
IHC	Immunohistochemistry
IF	Immunofluorescence
TMA	Tissue microarray
TGCA	The Cancer Genome Atlas
GEO	Gene Expression Omnibus
DEGs	Differential Expressed Genes
GO	Gene Ontology
MsigDB	Molecular signature database
GSEA	Gene set enrichment analysis
RNA-seq	RNA sequencing
scRNA-seq	Single-cell RNA sequencing

Supplementary Information

The online version contains supplementary material available at https://doi.org/10.1186/s12943-025-02293-y.

Supplementary Material 1.

Supplementary Material 2.

Acknowledgements
We thank Drs. Maruyama and Okumura of Abwiz Bio, San Diego, CA, for generating and characterizing the p53(K382me1) monoclonal antibody through their optimized phage display method. We are grateful to Sharlyn J. Mazur for insightful comments and to Irene Pillitteri for technical assistance.

Authors' contributions
V.V., F.V., G.S. and M.T. designed the experiments. V.V., G.S. and M.T. drafted the manuscript. V.V., F.V., S.D.B, D.L.P. and M.T. generated the figures. M.T. and C.D. developed and/or performed the IF and IHC analyses. V.L.L. provided samples of IBD and CRC patients. V.V., F.V., A.T., M.G. and C.M. performed animal studies. V.V., F.V., L.R.M and P.B. performed in vitro functional assays and generated stable shSETD8 CR-CSphC lines. G.P. performed qRT-PCR assays. V.V., F.V. and O.R.B. performed Western blotting and experiments for RNA-seq analysis. S.D.F and S.D.B. analyzed and elaborated data and performed statistical analysis. M.L.I. performed cytofluorimetry analyses. P.M. and K.B. performed and analyzed the ChIP assay. I.S., E.S., P.F. and S.D.B. analyzed the bulk RNA-seq data. D.L.P. analyzed the scRNA-seq data and the predicted cytokine secretion. K.B. and E.A. provided unique reagents, and with G.G. critically edited the manuscript. All authors reviewed the manuscript.

Authors' information
Giorgio Stassi and Veronica Veschi are co-corresponding authors. Giorgio Stassi and Matilde Todaro contributed equally to this work as last authors. Veronica Veschi and Francesco Verona contributed equally to this work as co-first authors.

Funding
V.V. and G.G. belong to the Department of Molecular Medicine, Dipartimento Eccellenza Italian Ministry of Education, Universities and Research – Dipartimenti di Eccellenza – L. 232/2016. The research leading to these results has received funding from PRIN 2022J8X7PJ project to S.D.F and from Department MePreCC- PJ_PROGRIC2023_MIS1B project to M.G. The research leading to these results has received funding by the European Union – NextGenerationEU – MIUR D.M. 737/2021 – research project entitled: "Ruolo di MERTK nell'interazione tra cellule tumorali e il microambiente nella progression del tumore alla mammella" to M.G., European Union – NextGenerationEU – MIUR D.M. 737/2021 – research project entitled: "Sviluppo di terapie innovative nel trattamento del carcinoma alla mammella" to A.T., European Union – FESR FSE PON Ricerca e Innovazione 2014–2020 DM 1062/2021 to C.M. and M.L.I., European Union – NextGenerationEU initiative under the Italian Ministry of University and Research as a part of the PNRR – M4C2-I1.3 Project PE00000019 'HEAL ITALIA' CUP B73C22001250006 to S.D.B, M.T., S.D.F. and G.S., and CUP B53C22004000006 to G.G., Fondo Finalizzato di Ateneo (FFR) – 2024 to A.T., C.M., M.L.I., S.D.B. and M.G. The research leading to these results has received funding from PSN2015, 6.2, CUP176J17000470001 project and PNRR-MAD-2022–12376183 project to M.T. The research leading to these results has received funding from PNRR-MAD-2022–12376835 project to G.S. and S.D.F. The research leading to these results has received funding from AIRC IG (21445) to G.S., AIRC IG (30306) to M.T. and AIRC IG (24329) to G.G. The work was in part supported by the Center for Cancer Research, NCI, NIH.

Data availability
The RNA-seq data generated in this study are publicly available in Gene Expression Omnibus (GEO) at GSE262144, and within the article and its supplementary data files.

Declarations

Ethics approval and consent to participate
CRC human tissues were harvested in accordance with the ethical standards of the Institutional Committee on Human Experimentation (authorization CE9/2015, Policlinico Paolo Giaccone, Palermo), with informed consent from the patients.
All animal experiments and procedures were approved and performed in accordance with the guidelines of the institutional animal care committee at the University of Palermo (authorization # n. 154/2017-PR, Italian Ministry of Health).

Consent for publication
All the authors provided consent for the publication of the manuscript in the journal *Molecular Cancer*.

Competing interests
The authors declare no competing interests.

Author details
[1]Department of Precision Medicine in Medical, Surgical and Critical Care, University of Palermo, Palermo 90127, Italy. [2]Department of Molecular Medicine, University of Rome La Sapienza, Rome 00161, Italy. [3]Department of Health Promotion Sciences, Internal Medicine and Medical Specialties (PROMISE), University of Palermo, Palermo 90127, Italy. [4]Villa Sofia-Cervello Hospital, Palermo 90146, Italy. [5]Clinical Trial Center, Biostatistics and Bioinformatics Unit, IRCCS - Regina Elena National Cancer Institute, Rome 00144, Italy. [6]Centre for Experimental Medicine and Rheumatology, the London School of Medicine and Dentistry, William Harvey Research Institute, Queen Mary University of London, Bartsand, London, UK. [7]Genome Analysis Unit, National Cancer Institute, National Institutes of Health, Bethesda, MD 20892, USA. [8]Chemical Immunology Section, Laboratory of Cell Biology, National Cancer Institute, Bethesda, MD, USA. [9]Istituto Pasteur-Fondazione Cenci Bolognetti, University of Rome La Sapienza, Rome 00161, Italy. [10]Azienda Ospedaliera Universitaria Policlinico "Paolo Giaccone" (AOUP), Palermo, Italy.

Received: 14 June 2024 Accepted: 5 March 2025
Published online: 31 March 2025

References

1. Siegel RL, Miller KD, Fedewa SA, Ahnen DJ, Meester RGS, Barzi A, Jemal A. Colorectal cancer statistics, 2017. CA Cancer J Clin. 2017;67:177–93.
2. Hollstein M, Sidransky D, Vogelstein B, Harris CC. p53 mutations in human cancers. Science. 1991;253:49–53.
3. Cooks T, Pateras IS, Tarcic O, Solomon H, Schetter AJ, Wilder S, Lozano G, Pikarsky E, Forshew T, Rosenfeld N, et al. Mutant p53 prolongs NF-kappaB activation and promotes chronic inflammation and inflammation-associated colorectal cancer. Cancer Cell. 2013;23:634–46.
4. Lu M, Breyssens H, Salter V, Zhong S, Hu Y, Baer C, Ratnayaka I, Sullivan A, Brown NR, Endicott J, et al. Restoring p53 Function in Human Melanoma

Cells by Inhibiting MDM2 and Cyclin B1/CDK1-Phosphorylated Nuclear iASPP. Cancer Cell. 2016;30:822–3.
5. Veschi V, Liu Z, Voss TC, Ozbun L, Gryder B, Yan C, Hu Y, Ma A, Jin J, Mazur SJ, et al. Epigenetic siRNA and Chemical Screens Identify SETD8 Inhibition as a Therapeutic Strategy for p53 Activation in High-Risk Neuroblastoma. Cancer Cell. 2017;31:50–63.
6. Beck DB, Oda H, Shen SS, Reinberg D. PR-Set7 and H4K20me1: at the crossroads of genome integrity, cell cycle, chromosome condensation, and transcription. Genes Dev. 2012;26:325–37.
7. Takawa M, Cho HS, Hayami S, Toyokawa G, Kogure M, Yamane Y, Iwai Y, Maejima K, Ueda K, Masuda A, et al. Histone lysine methyltransferase SETD8 promotes carcinogenesis by deregulating PCNA expression. Cancer Res. 2012;72:3217–27.
8. Schnepp RW, Khurana P, Attiyeh EF, Raman P, Chodosh SE, Oldridge DA, Gagliardi ME, Conkrite KL, Asgharzadeh S, Seeger RC, et al. A LIN28B-RAN-AURKA Signaling Network Promotes Neuroblastoma Tumorigenesis. Cancer Cell. 2015;28:599–609.
9. Shi X, Kachirskaia I, Yamaguchi H, West LE, Wen H, Wang EW, Dutta S, Appella E, Gozani O. Modulation of p53 function by SET8-mediated methylation at lysine 382. Mol Cell. 2007;27:636–46.
10. Kukita A, Sone K, Kaneko S, Kawakami E, Oki S, Kojima M, Wada M, Toyohara Y, Takahashi Y, Inoue F, et al. The Histone Methyltransferase SETD8 Regulates the Expression of Tumor Suppressor Genes via H4K20 Methylation and the p53 Signaling Pathway in Endometrial Cancer Cells. Cancers (Basel). 2022;14:5367–86.
11. Tuzon CT, Spektor T, Kong X, Congdon LM, Wu S, Schotta G, Yokomori K, Rice JC. Concerted activities of distinct H4K20 methyltransferases at DNA double-strand breaks regulate 53BP1 nucleation and NHEJ-directed repair. Cell Rep. 2014;8:430–8.
12. Xu L, Zhang L, Sun J, Hu X, Kalvakolanu DV, Ren H, Guo B. Roles for the methyltransferase SETD8 in DNA damage repair. Clin Epigenetics. 2022;14:34.
13. Yin Y, Yao S, Hu Y, Feng Y, Li M, Bian Z, Zhang J, Qin Y, Qi X, Zhou L, et al. The Immune-microenvironment Confers Chemoresistance of Colorectal Cancer through Macrophage-Derived IL6. Clin Cancer Res. 2017;23:7375–87.
14. De Sousa EMF, Wang X, Jansen M, Fessler E, Trinh A, de Rooij LP, de Jong JH, de Boer OJ, van Leersum R, Bijlsma MF, et al. Poor-prognosis colon cancer is defined by a molecularly distinct subtype and develops from serrated precursor lesions. Nat Med. 2013;19:614–8.
15. Thanki K, Nicholls ME, Gajjar A, Senagore AJ, Qiu S, Szabo C, Hellmich MR, Chao C. Consensus Molecular Subtypes of Colorectal Cancer and their Clinical Implications. Int Biol Biomed J. 2017;3:105–11.
16. Suva ML, Riggi N, Bernstein BE. Epigenetic reprogramming in cancer. Science. 2013;339:1567–70.
17. Solomon H, Dinowitz N, Pateras IS, Cooks T, Shetzer Y, Molchadsky A, Charni M, Rabani S, Koifman G, Tarcic O, et al. Mutant p53 gain of function underlies high expression levels of colorectal cancer stem cells markers. Oncogene. 2018;37:1669–84.
18. Matas D, Milyavsky M, Shats I, Nissim L, Goldfinger N, Rotter V. p53 is a regulator of macrophage differentiation. Cell Death Differ. 2004;11:458–67.
19. Li L, Ng DS, Mah WC, Almeida FF, Rahmat SA, Rao VK, Leow SC, Laudisi F, Peh MT, Goh AM, et al. A unique role for p53 in the regulation of M2 macrophage polarization. Cell Death Differ. 2015;22:1081–93.
20. Zhou Y, Que KT, Zhang Z, Yi ZJ, Zhao PX, You Y, Gong JP, Liu ZJ. Iron overloaded polarizes macrophage to proinflammation phenotype through ROS/acetyl-p53 pathway. Cancer Med. 2018;7:4012–22.
21. He XY, Xiang C, Zhang CX, Xie YY, Chen L, Zhang GX, Lu Y, Liu G. p53 in the Myeloid Lineage Modulates an Inflammatory Microenvironment Limiting Initiation and Invasion of Intestinal Tumors. Cell Rep. 2015;13:888–97.
22. Larionova I, Kazakova E, Patysheva M, Kzhyshkowska J. Transcriptional, Epigenetic and Metabolic Programming of Tumor-Associated Macrophages. Cancers (Basel). 2020;12:1411–52.
23. Zhou RW, Harpaz N, Itzkowitz SH, Parsons RE. Molecular mechanisms in colitis-associated colorectal cancer. Oncogenesis. 2023;12:48.
24. Genin M, Clement F, Fattaccioli A, Raes M, Michiels C. M1 and M2 macrophages derived from THP-1 cells differentially modulate the response of cancer cells to etoposide. BMC Cancer. 2015;15:577.
25. Li Z, Nie F, Wang S, Li L. Histone H4 Lys 20 monomethylation by histone methylase SET8 mediates Wnt target gene activation. Proc Natl Acad Sci U S A. 2011;108:3116–23.
26. Todaro M, Gaggianesi M, Catalano V, Benfante A, Iovino F, Biffoni M, Apuzzo T, Sperduti I, Volpe S, Cocorullo G, et al. CD44v6 is a marker of constitutive and reprogrammed cancer stem cells driving colon cancer metastasis. Cell Stem Cell. 2014;14:342–56.
27. Baker AM, Cross W, Curtius K, Al Bakir I, Choi CR, Davis HL, Temko D, Biswas S, Martinez P, Williams MJ, et al. Evolutionary history of human colitis-associated colorectal cancer. Gut. 2019;68:985–95.
28. Jess T, Rungoe C, Peyrin-Biroulet L. Risk of colorectal cancer in patients with ulcerative colitis: a meta-analysis of population-based cohort studies. Clin Gastroenterol Hepatol. 2012;10:639–45.
29. Di Franco S, Bianca P, Sardina DS, Turdo A, Gaggianesi M, Veschi V, Nicotra A, Mangiapane LR, Lo Iacono M, Pillitteri I, et al. Adipose stem cell niche reprograms the colorectal cancer stem cell metastatic machinery. Nat Commun. 2021;12:5006.
30. Ko CY, Chang WC, Wang JM. Biological roles of CCAAT/Enhancer-binding protein delta during inflammation. J Biomed Sci. 2015;22:6.
31. Balamurugan K, Sterneck E. The many faces of C/EBPdelta and their relevance for inflammation and cancer. Int J Biol Sci. 2013;9:917–33.
32. Hartl L, Duitman J, Bijlsma MF, Spek CA. The dual role of C/EBPdelta in cancer. Crit Rev Oncol Hematol. 2023;185:103983.
33. Pendse M, De Selle H, Vo N, Quinn G, Dende C, Li Y, Salinas CN, Srinivasan T, Propheter DC, Crofts AA, et al. Macrophages regulate gastrointestinal motility through complement component 1q. Elife. 2023;12:1–30.
34. Ma A, Yu W, Li F, Bleich RM, Herold JM, Butler KV, Norris JL, Korboukh V, Tripathy A, Janzen WP, et al. Discovery of a selective, substrate-competitive inhibitor of the lysine methyltransferase SETD8. J Med Chem. 2014;57:6822–33.
35. Huang J, Sengupta R, Espejo AB, Lee MG, Dorsey JA, Richter M, Opravil S, Shiekhattar R, Bedford MT, Jenuwein T, Berger SL. p53 is regulated by the lysine demethylase LSD1. Nature. 2007;449:105–8.
36. Antona A, Leo G, Favero F, Varalda M, Venetucci J, Faletti S, Todaro M, Mazzucco E, Soligo E, Saglietti C, et al. Targeting lysine-specific demethylase 1 (KDM1A/LSD1) impairs colorectal cancer tumorigenesis by affecting cancer cells stemness, motility, and differentiation. Cell Death Discov. 2023;9:201.
37. Liu M, Shi Y, Hu Q, Qin Y, Ji S, Liu W, Zhuo Q, Fan G, Ye Z, Song C, et al. SETD8 induces stemness and epithelial-mesenchymal transition of pancreatic cancer cells by regulating ROR1 expression. Acta Biochim Biophys Sin (Shanghai). 2021;53:1614–24.
38. Piao L, Che N, Li H, Li M, Feng Y, Liu X, Kim S, Jin Y, Xuan Y. SETD8 promotes stemness characteristics and is a potential prognostic biomarker of gastric adenocarcinoma. Exp Mol Pathol. 2020;117: 104560.
39. Piao L, Feng Y, Che N, Li M, Li X, Jin Y, Xuan Y. SETD8 is a prognostic biomarker that contributes to stem-like cell properties in non-small cell lung cancer. Pathol Res Pract. 2020;216: 153258.
40. Scott MT, Liu W, Mitchell R, Clarke CJ, Kinstrie R, Warren F, Almasoudi H, Stevens T, Dunn K, Pritchard J, et al. Activating p53 abolishes self-renewal of quiescent leukaemic stem cells in residual CML disease. Nat Commun. 2024;15:651.
41. Ghatak D, Das Ghosh D, Roychoudhury S. Cancer Stemness: p53 at the Wheel. Front Oncol. 2020;10: 604124.
42. Shi D, Jiang P. A Different Facet of p53 Function: Regulation of Immunity and Inflammation During Tumor Development. Front Cell Dev Biol. 2021;9: 762651.
43. Qian BZ, Pollard JW. Macrophage diversity enhances tumor progression and metastasis. Cell. 2010;141:39–51.
44. Sharma VP, Tang B, Wang Y, Duran CL, Karagiannis GS, Xue EA, Entenberg D, Borriello L, Coste A, Eddy RJ, et al. Live tumor imaging shows macrophage induction and TMEM-mediated enrichment of cancer stem cells during metastatic dissemination. Nat Commun. 2021;12:7300.
45. Shin AE, Tesfagiorgis Y, Larsen F, Derouet M, Zeng PYF, Good HJ, Zhang L, Rubinstein MR, Han YW, Kerfoot SM, et al. F4/80(+)Ly6C(high) Macrophages Lead to Cell Plasticity and Cancer Initiation in Colitis. Gastroenterology. 2023;164(593–609): e513.
46. Mantovani A, Marchesi F, Malesci A, Laghi L, Allavena P. Tumour-associated macrophages as treatment targets in oncology. Nat Rev Clin Oncol. 2017;14:399–416.

47. Verhagen MP, Joosten R, Schmitt M, Välimäki N, Sacchetti A, Rajamäki K, Choi J, Procopio P, Silva S, van der Steen B, van den Bosch TPP, Seinstra D, de Vries AC, Doukas M, Augenlicht LH, Aaltonen LA, Fodde R. Non-stem cell lineages as an alternative origin of intestinal tumorigenesis in the context of inflammation. Nat Genet. 2024;56(7):1456-67. https://doi.org/10.1038/s41588-024-01801-y.
48. Wang T, Song P, Zhong T, Wang X, Xiang X, Liu Q, Chen H, Xia T, Liu H, Niu Y, et al. The inflammatory cytokine IL-6 induces FRA1 deacetylation promoting colorectal cancer stem-like properties. Oncogene. 2019;38:4932–47.
49. Bharti R, Dey G, Mandal M. Cancer development, chemoresistance, epithelial to mesenchymal transition and stem cells: A snapshot of IL-6 mediated involvement. Cancer Lett. 2016;375:51–61.
50. Rokavec M, Oner MG, Li H, Jackstadt R, Jiang L, Lodygin D, Kaller M, Horst D, Ziegler PK, Schwitalla S, et al. IL-6R/STAT3/miR-34a feedback loop promotes EMT-mediated colorectal cancer invasion and metastasis. J Clin Invest. 2014;124:1853–67.
51. Wei C, Yang C, Wang S, Shi D, Zhang C, Lin X, Liu Q, Dou R, Xiong B. Crosstalk between cancer cells and tumor associated macrophages is required for mesenchymal circulating tumor cell-mediated colorectal cancer metastasis. Mol Cancer. 2019;18:64.
52. Hosaka K, Rojas K, Fazal HZ, Schneider MB, Shores J, Federico V, McCord M, Lin L, Hoh B. Monocyte Chemotactic Protein-1-Interleukin-6-Osteopontin Pathway of Intra-Aneurysmal Tissue Healing. Stroke. 2017;48:1052–60.
53. Yang LX, Zhang CT, Yang MY, Zhang XH, Liu HC, Luo CH, Jiang Y, Wang ZM, Yang ZY, Shi ZP, et al. C1Q labels a highly aggressive macrophage-like leukemia population indicating extramedullary infiltration and relapse. Blood. 2023;141:766–86.
54. Kim KB, Yi JS, Nguyen N, Lee JH, Kwon YC, Ahn BY, Cho H, Kim YK, Yoo HJ, Lee JS, Ko YG. Cell-surface receptor for complement component C1q (gC1qR) is a key regulator for lamellipodia formation and cancer metastasis. J Biol Chem. 2011;286:23093–101.
55. Iwasaki M, Liedtke M, Gentles AJ, Cleary ML. CD93 Marks a Non-Quiescent Human Leukemia Stem Cell Population and Is Required for Development of MLL-Rearranged Acute Myeloid Leukemia. Cell Stem Cell. 2015;17:412–21.
56. Aizaz M, Khan A, Khan F, Khan M, Musad Saleh EA, Nisar M, Baran N. The cross-talk between macrophages and tumor cells as a target for cancer treatment. Front Oncol. 2023;13:1259034.
57. Hassin O, Oren M. Drugging p53 in cancer: one protein, many targets. Nat Rev Drug Discov. 2023;22:127–44.

Publisher's Note